

1 **Evolution of dissolved and particulate chromophoric materials during the**
2 **VAHINE mesocosm experiment in the New Caledonian coral lagoon (South**
3 **West Pacific)**

4

5 M. Tedetti^{1*}, L. Marie^{1,2}, R. Röttgers³, M. Rodier⁴, F. Van Wambeke¹, S. Helias¹, M.
6 Caffin¹, V. Cornet-Barthaux¹, and C. Dupouy¹

7

8 ¹ Aix Marseille Université, CNRS/INSU, Université de Toulon, IRD, Mediterranean Institute
9 of Oceanography (MIO) UM 110, 13288, Marseille, France

10 ² Present affiliation: Université de Bretagne Occidentale, IUEM, Lemar UMR CNRS 6539,
11 Place Copernic, F-29280 Plouzané, France

12 ³ Helmholtz-Zentrum Geesthacht, Centre for Materials and Coastal Research, Institute for
13 Coastal Research, Remote Sensing, Geesthacht, Germany

14 ⁴ IRD, Université de la Polynésie française - Institut Malardé - Ifremer, UMR 241,
15 Ecosystèmes Insulaires Océaniques (EIO), IRD Tahiti, PB 529, 98713 Papeete, Tahiti, French
16 Polynesia

17

18 * Corresponding author: marc.tedetti@mio.osupytheas.fr; Phone: + 33 (0)4 86 09 05 27;

19 Fax: + 33 (0)4 91 82 96 41

20

21 For submission to Biogeosciences as a research article for the special issue “Biogeochemical
22 and biological response to a diazotroph bloom in a low-nutrient, low-chlorophyll ecosystem:
23 results from the VAHINE mesocosms experiment”

24

25 Revised version 06 May 2016

26 **Abstract**

27 In the framework of the VAHINE project, we investigated the spectral characteristics
28 and the variability of dissolved and particulate chromophoric materials throughout a 23-day
29 mesocosm experiment conducted in the South West Pacific at the exit of the New Caledonian
30 coral lagoon (22°29.073 S - 166°26.905 E) from January 13th to February 4th 2013. Samples
31 were collected in a mesocosm fertilized with phosphorus at 1, 6 and 12 m depth and in the
32 surrounding waters. Light absorption coefficients of chromophoric dissolved organic matter
33 (CDOM) [$a_g(\lambda)$] and particulate matter [$a_p(\lambda)$] were determined using a point-source
34 integrating-cavity absorption meter (PSICAM), while fluorescent DOM (FDOM) components
35 were determined from excitation-emission matrices (EEMs) combined with parallel factor
36 analysis (PARAFAC). The evolutions of $a_g(\lambda)$ and $a_p(\lambda)$ in the mesocosm were similar to
37 those of total chlorophyll *a* concentration, *Synechococcus* spp. and picoeukaryote abundances,
38 bacterial production, particulate organic nitrogen and total organic carbon concentrations,
39 with roughly a decrease from the beginning of the experiment to days 9-10, and an increase
40 from days 9-10 to the end of the experiment. In the surrounding waters, the same trend was
41 observed but the increase was much less pronounced, emphasizing the effect of the
42 phosphorus fertilization on the mesocosm's plankton community. Correlations suggested that
43 both *Synechococcus* cyanobacteria and heterotrophic bacteria were strongly involved in the
44 production of CDOM and absorption of particulate matter. The increase in phytoplankton
45 biomass during the second part of the experiment led to a higher contribution of particulate
46 material in the absorption budget at 442 nm. The three FDOM components identified
47 (tryptophan-, tyrosine- and UVC humic-like fluorophores) did not follow the evolution of
48 CDOM and particulate matter, suggesting they were driven by different
49 production/degradation processes. Finally, the results of this work support the idea there is

50 indirect coupling between the dynamics of N₂ fixation and that of chromophoric material *via*
51 the stimulation of *Synechococcus* bloom.

52

53 **Key words:** South West Pacific, mesocosm, CDOM, FDOM, particulate absorption,
54 cyanobacteria.

55

56

57

58

59

60

61

62

63

64

65

66

67

68

69

70

71

72

73

74

75 **1. Introduction**

76

77 Besides water itself, light absorption in the marine environment is due to three main
78 biogeochemical constituents: 1) chromophoric dissolved organic matter (CDOM), also known
79 as gelbstoff, gilvin and yellow substances, and chromophoric particulate matter, subdivided
80 into 2) phytoplankton (photoautotrophic microorganisms), composed of both prokaryotic
81 (cyanobacteria) and eukaryotic species (diatoms, dinoflagellates, coccolithophores,...), and 3)
82 non algal particles (NAP), comprising organic and minerogenic detritus, and heterotrophic
83 organisms. Absorption spectra of CDOM, phytoplankton and NAP have been extensively
84 studied over the last two decades in various oceanic provinces including coastal waters and
85 open ocean (Blough and Del Vecchio, 2002; Babin et al., 2003; Bricaud et al., 2010;
86 Matsuoka et al., 2014). Indeed, in addition to their key role in the oceanic carbon cycle, these
87 three constituents strongly influence the underwater light field and the apparent optical
88 properties of seawater. The knowledge of their absorption spectra is thus essential for bio-
89 optical modeling and remote sensing applications but can be used as well to investigate
90 biological processes in the ocean.

91 Absorption coefficients of CDOM [$a_g(\lambda)$] and NAP [$a_{nap}(\lambda)$] typically decrease
92 monotonically (exponentially) from ultraviolet (UV, 280-400 nm) to visible (400-700 nm)
93 wavelengths (Nelson et al., 1998; Swan et al., 2009; Tilstone et al., 2012). Even though
94 CDOM absorption spectra are usually featureless, some “shoulders” have been observed
95 sporadically in the UV and visible spectral domains and attributed to the presence of
96 dissolved absorbing pigments released by phytoplankton cells: mycosporine-like amino acids
97 (MAAs) at 310-320 nm or at 330-360 nm, and phaeopigments or non-chlorin metal-free
98 porphyrins at 410-420 nm (Whitehead and Vernet, 2000; Röttgers and Koch, 2012; Organelli
99 et al., 2014; Pavlov et al., 2014). In contrast, absorption coefficients of phytoplankton [$a_\phi(\lambda)$]

100 determined from natural samples commonly display two main peaks in the visible range,
101 around 435-450 and 675 nm, attributable to its content in total chlorophyll *a* (TChl *a* = mono
102 Chl *a* + divinyl Chl *a*) (Lutz et al., 1996; Dupouy et al., 1997; Bricaud et al., 2004), but may
103 also reveal other peaks or shoulders resulting from the presence of other pigments: MAAs at
104 325 nm (Bricaud et al., 2010), TChl *b*, TChl *c* and photoprotective carotenoids at 460-470 nm,
105 photosynthetic carotenoids and photoprotective keto-carotenoids at 490 nm (Carreto, 1985;
106 Stuart et al., 1998; Wozniak et al., 1999; Lohrenz et al., 2003) as well as phycoerythrin at 550
107 nm (Morel, 1997). Hence, while chromophoric detrital matter (CDM = CDOM + NAP) is the
108 major contributor to total absorption in the UV domain (~ 60-95 %), in the blue region (440-
109 490 nm), the contributions of CDM and phytoplankton tend to be equivalent (~ 40-50 %),
110 while CDOM alone is accounting for ~ 80-95 % of CDM in the UV and blue ranges (Siegel et
111 al., 2002; 2005; Tedetti et al., 2010; Nelson and Siegel, 2013).

112 In “Case 1 waters” (Morel and Prieur, 1977), which are generally - but not necessarily -
113 open ocean clear waters, optical properties are controlled by phytoplankton and all its derived
114 material, and TChl *a* concentration may be utilized as an index of optical properties thanks to
115 its covariation with $a_{\phi}(\lambda)$, $a_g(\lambda)$, $a_{\text{nap}}(\lambda)$ and particulate backscattering coefficient [$b_{\text{bp}}(\lambda)$]
116 (Antoine et al., 2014). Due to the covariation with $a_{\phi}(\lambda)$ in Case 1 waters, CDOM is
117 considered as being a by-product of phytoplanktonic production. Nonetheless, recent studies
118 have highlighted some degree of de-phasing between the dynamics in phytoplankton and that
119 of CDOM at the global, regional or seasonal scale (Siegel et al., 2002; Morel et al., 2010;
120 Xing et al., 2014). Whilst photobleaching is now considered as a major degradation process of
121 CDOM in surface waters (Del Vecchio and Blough, 2002; Helms et al., 2008; Bracchini et al.,
122 2010; Swan et al., 2012), the main source of CDOM in open ocean is still a matter of debate,
123 particularly for its “humic-like” component, which absorbs light over a broad range of UV
124 and visible wavelengths and fluoresces in the visible domain (Andrew et al., 2013). Some

125 works suggest that this humic-like CDOM is in part a remainder of terrestrial matter that has
126 been diluted and transformed during transit to and within the ocean (Blough and Del Vecchio,
127 2002; Hernes and Benner, 2006; Murphy et al., 2008; Andrew et al., 2013). Conversely, other
128 studies put forward its autochthonous marine source and its production from phytoplankton,
129 including green algal, diatoms, dinoflagellates (Vernet and Whitehead, 1996; Romera-Castillo
130 et al., 2010; 2011; Chari et al., 2013), the diazotrophic (N₂-fixing) cyanobacteria
131 *Trichodesmium* spp. (Subramaniam et al., 1999; Steinberg et al., 2004) and the non-
132 diazotrophic picocyanobacteria *Synechococcus* spp. and *Prochlorococcus* spp. (Romera-
133 Castillo et al., 2011), from zooplankton (Steinberg et al., 2004; Ortega-Retuerta et al., 2009),
134 or from the bacterial degradation (mineralization) of phytoplankton-derived organic matter
135 (Nelson et al., 1998; 2010; Swan et al., 2009).

136 The New Caledonian coral lagoon, located in the South West Pacific, is a tropical,
137 oligotrophic Low Nutrient Low Chlorophyll (LNLC) ecosystem in which diazotrophs such as
138 cyanobacteria *Trichodesmium* spp. (Dupouy et al., 1988; 2008; Masotti et al., 2007; Rodier
139 and Le Borgne, 2010) and diazotrophic picocyanobacteria (Biegala and Raimbault, 2008) but
140 also non-diazotrophic picocyanobacteria such as *Synechococcus* spp. and *Prochlorococcus*
141 spp. (Biegala and Raimbault, 2008; Neveux et al., 2009) play a significant role. Although the
142 biogeochemical conditions in the New Caledonian coral lagoon are well documented for
143 several years (see review by Grenz et al., 2010), the dynamics of CDOM remains poorly
144 known in this environment. In the framework of the VARIability of vertical and troPHic
145 transfer of fixed N₂ in the south wEst Pacific (VAHINE) mesocosm experiment, the
146 objectives of the present study were 1) to assess the spectral characteristics and the variability
147 of dissolved and particulate chromophoric materials throughout a 23-day mesocosm
148 experiment, and 2) to tentatively identify the main biogeochemical contributors (diazotrophic
149 and non-diazotrophic primary producers, heterotrophic bacteria) driving changes in

150 chromophoric material over the course of the experiment. Chromophoric parameters we
151 examined here were absorption coefficients of CDOM [$a_g(\lambda)$] and particulate matter [$a_p(\lambda) =$
152 $a_\phi(\lambda) + a_{\text{nap}}(\lambda)$], determined over the spectral domain 370-720 nm, the spectral slope of
153 CDOM (S_g), computed over the range 370-500 nm, as well as fluorescent DOM (FDOM)
154 components, determined from excitation-emission matrices (EEMs) combined with parallel
155 factor analysis (PARAFAC).

156

157 **2. Material and methods**

158

159 **2.1. The mesocosm experiment**

160 *Study site and mesocosm description.* The VAHINE mesocosm experiment was
161 conducted from January 13th to February 4th, 2013 in the South West Pacific at an exit of the
162 New Caledonian coral lagoon, 28 km off the coast of New Caledonia (22°29.073 S -
163 166°26.905 E) (Fig. 1). At the deployment site the water depth was 25 m and the bottom was
164 sandy. The site was protected by land from the dominant trade winds (SE sector) and
165 characterized by high influence of oceanic oligotrophic waters coming from outside the
166 lagoon through the Boulari passage (Ouillon et al., 2010). Three large mesocosms (hereafter
167 called M1, M2 and M3), of 50 m³ volume each, were deployed (Fig. 2). All details
168 concerning the mesocosm design and deployment are given in Bonnet et al. (2015). In brief,
169 the mesocosms consisted in large cylindrical bags made of one polyethylene film and one
170 ethylene vinyl acetate (EVA, 19 %) film, each 500 μm thick, with nylon meshing in between
171 to allow maximum resistance and light penetration. They were 2.3 m in diameter, 15 m in
172 depth and were equipped with removable sediment traps allowing collection of sinking
173 material. The top of the bags were maintained 1 m above the surface with floats to prevent
174 inflow of external water. Their straightness was maintained by weights at the bottom of the

175 mesocosms. Before starting sampling, the mesocosms were left opened from the bottom for
176 24 h to insure a total homogeneity of the water column.

177 ***Nutrient fertilization.*** To prevent phosphate limitation, the mesocosms were fertilized in
178 the evening of day 4 with dissolved inorganic phosphorus (DIP) to a final concentration of 0.8
179 μM (see details of the fertilization procedure in Bonnet et al., 2015). This phosphate
180 fertilization aimed at stimulating diazotroph activities.

181 ***Sampling and in situ measurements.*** During the 23 days of the experiment, seawater
182 sampling was performed every morning from a 4 m² floating platform at three depths (1, 6
183 and 12 m) in each mesocosm and at 1 m depth in the surrounding waters close to the
184 mesocosm (“OUT”) using a compressed air-driven, metal-free pump (AstiPure™) connected
185 to a polyethylene tubing. Samples were filled into 50-L polypropylene carboys and
186 immediately transported for subsampling and sample treatments onboard the R/V *Alis*,
187 moored 1 nautical mile away from the mesocosm site. Along with discrete sampling, vertical
188 profiles of temperature, salinity, Chl *a* fluorescence, turbidity and light intensity were
189 obtained daily (at 7 a.m. local time) in each mesocosm and in the surrounding waters using a
190 911plus conductivity temperature depth (CTD) profiler (Sea-Bird Electronics, Inc.). For our
191 specific parameters, i.e. dissolved and particulate chromophoric materials, we only sampled
192 the mesocosm M1 at 1, 6 and 12 m depth and the surrounding waters at 1 m depth.

193 ***Filtration.*** Onboard R/V *Alis*, samples for CDOM absorption and fluorescence
194 measurements were immediately filtered under low vacuum (< 50 mm Hg) through 0.2 μm
195 polycarbonate filters (25 mm diameter, Nuclepore) using small, pre-combusted (450 °C, 6 h)
196 glass filtration systems. Prior to sample filtration, the Nuclepore filters were cleaned by first
197 soaking them for several minutes in 1 M HCl, then in ultrapure water, and processing them by
198 filtering through and discarding 300 mL of ultrapure water and lastly 50 mL of sample. Then,
199 1 L of sample was filtered and the 0.2 μm filtrate transferred into pre-combusted Schott®

200 glass bottles for analyses. Powder-free disposable gloves were worn during sampling,
201 filtration and analyses to avoid sample contamination. All absorption coefficient
202 measurements [$a_g(\lambda)$ and $a_{g+p}(\lambda)$] were performed directly onboard (see section 2.2), while
203 samples for fluorescence measurements were stored at 4 °C in the dark for several days until
204 analyses.

205 ***The two phases of the experiment.*** In the results presented below, the 23-day mesocosm
206 experiment was separated into two periods: P1, from day 5 to day 14, and P2, from day 15 to
207 day 23. P1 and P2 denote the two phases of the experiment when the diazotrophic community
208 was dominated by diatom-diazotroph associations (DDAs), more specifically heterocyst-
209 forming *Richelia* associated with *Rhizosolenia*, and unicellular cyanobacteria group C
210 (UCYN-C), respectively (Berthelot et al., 2015; Turk-Kubo et al., 2015).

211

212 **2.2. Absorption of CDOM and particulate matter**

213 ***Measurement.*** Absorption coefficients of CDOM and CDOM + particulate matter
214 [$a_g(\lambda)$ and $a_{g+p}(\lambda)$] were determined by measuring absorption of 0.2 μm filtered and unfiltered
215 samples using a point-source integrating-cavity absorption meter (PSICAM) instrument as
216 described by Röttgers et al. (2007) and Röttgers and Doerffer (2007). The cavity of the
217 PSICAM was filled with purified water (Milli-Q water), air bubbles were removed from the
218 cavity wall and the central light sphere by gentle shaking, and a reference intensity spectrum
219 was recorded between 370 and 726 nm. Afterwards, sample water was poured into the cavity
220 in the same way, and a sample intensity spectrum was recorded. The cavity was rinsed and
221 filled with purified water again, and a second reference intensity spectrum was recorded. The
222 two reference spectra were used to calculate two “transmissions” (sample/reference) and,
223 further, two absorption coefficient spectra. The mean of these two spectra was taken as the
224 real absorption coefficient spectrum. The calibration of the PSICAM consisted of

225 determinations of the total cavity reflectivity spectrum by using solutions of the dye nigrosine
226 (Certistain[®], Merck) with maximum absorption between 1 and 3 m⁻¹. Absorption spectra were
227 corrected for salinity and temperature differences between sample and reference water
228 according to Röttgers and Doerffer (2007). The mean precision of the PSICAM within the
229 range 370-700 nm is ± 0.0008 m⁻¹, whereas its accuracy here is ± 2 %, even for absorption
230 values < 0.1 m⁻¹.

231 ***Particulate absorption and CDOM spectral slope determination.*** Absorption
232 coefficients of particulate matter [$a_p(\lambda)$] were determined by subtracting $a_g(\lambda)$ from $a_{g+p}(\lambda)$
233 over the range 370-720 nm. Spectral slope of $a_g(\lambda)$, S_g (in nm⁻¹), was computed by applying a
234 nonlinear (exponential), least-squares fit to the $a_g(\lambda)$ values between 370 and 500 nm in
235 accordance with the following formula:

$$236 \quad a_g(\lambda) = a_g(\lambda_0) \times e^{-S_g(\lambda-\lambda_0)}$$

237 The fit was conducted on raw (i.e. not log-transformed) data according to the
238 recommendations by Twardowski et al. (2004). The average correlation coefficient (r) of the
239 exponential least-squares fits was 1.00 ($n = 72$). The spectral range used here for the slope
240 determination (370-500 nm) was close to that employed in previous studies for different
241 oceanic waters (i.e. 350-500 nm) (Babin et al., 2003; Röttgers and Doerffer, 2007; Bricaud et
242 al., 2010; Para et al., 2010; Organelli et al., 2014).

243

244 **2.3. Fluorescence of DOM**

245 ***Measurements.*** FDOM measurements were performed on 0.2-µm filtered samples using
246 a Hitachi F-7000 spectrofluorometer. The correction of spectra for instrumental response was
247 conducted from 200 to 600 nm according to the procedure recommended by the manufacturer
248 (Hitachi F-7000 Instruction Manual) and fully described in Tedetti et al. (2012). The
249 excitation (Ex) and emission (Em) correction curves were applied internally by the instrument

250 to correct each fluorescence measurement acquired in signal over reference ratio mode. The
251 samples were allowed to reach room temperature in the dark and transferred into a 1-cm
252 pathlength far-UV transparent silica quartz cuvette (170-2600 nm; LEADER LAB). The
253 sample in the cuvette was kept at 20 °C inside the instrument using a circulating water bath
254 connected to the cell holder. The cuvette was cleaned with 1 M HCl and ultrapure water, and
255 triple rinsed with the sample before use. EEMs were generated over λ_{Ex} between 200 and 500
256 nm in 5-nm intervals, and λ_{Em} between 280 and 550 nm in 2-nm intervals, with 5-nm slit
257 widths on both Ex and Em sides, a scan speed of 1200 nm min⁻¹, a time response of 0.5 s and
258 a PMT voltage of 700 V. Blanks (ultrapure water) and solutions of 0.1 to 10 $\mu\text{g L}^{-1}$ quinine
259 sulphate dihydrate (Fluka, purum for fluorescence) in 0.05 M sulphuric acid were run with
260 each set of samples. Two replicates were run for each sample.

261 ***Fluorescence data processing.*** Different processing steps were carried out on the
262 fluorescence data: 1) all the fluorescence data were normalized to the intensity of the
263 ultrapure water Raman scatter peak at $\lambda_{\text{Ex}}/\lambda_{\text{Em}}$ of 275/303 nm, measured daily as an internal
264 standard (Coble, 1996). This value varied by 4 % ($n = 20$). 2) The mean, normalized EEM of
265 ultrapure water was subtracted from normalized sample EEMs to eliminate the water Raman
266 scatter signal. 3) These blank-corrected sample EEMs were converted into quinine sulphate
267 unit (QSU), where 1 QSU corresponded to the fluorescence of 1 $\mu\text{g L}^{-1}$ quinine sulphate at
268 $\lambda_{\text{Ex}}/\lambda_{\text{Em}}$ of 350/450 nm (5-nm slit widths) (Coble, 1996; Murphy et al., 2008). The conversion
269 in QSU was made by dividing each EEM fluorescence data by the mean slope of a linear
270 regression of fluorescence *vs.* concentration for the different quinine sulphate solutions (i.e.
271 8.4 arbitrary fluorescence intensity units/QSU). r values of these linear regressions were on
272 average 0.99 and the detection and quantification limits of the fluorescence measurements
273 were 0.19 and 0.63 QSU, respectively. The water Raman scatter peak was integrated from λ_{Em}
274 380 to 426 nm at λ_{Ex} of 350 nm for ultrapure water samples. The mean value was used to

275 establish a conversion factor between QSU and Raman unit (RU, nm⁻¹), based on the Raman-
276 area normalized slope of the quinine sulphate linear regression. The conversion factor was
277 0.025 RU per QSU. Considering the low $a_g(\lambda)$ values, samples were not corrected for inner
278 filter effects (Stedmon and Bro, 2008).

279

280 **2.4. Parallel factor analysis (PARAFAC)**

281 In this work, a PARAFAC model was created and validated for 130 calibrated EEMs
282 according to the method by Stedmon et al. (2003). The EEM wavelength ranges used were
283 210-500 and 280-550 nm for Ex and Em, respectively. EEMs were merged into a three-
284 dimensional data array of the form: 130 samples \times 59 λ_{EX} \times 136 λ_{EM} . The PARAFAC program
285 was executed using the DOMFluor toolbox v1.6 (Stedmon and Bro, 2008) running under
286 MATLAB[®] 7.10.0 (R2010a). The full analysis showed that no outliers were present in the
287 dataset. The validation of the PARAFAC model (running with the non-negativity constraint)
288 and the determination of the correct number of components (from 2 to 6 components tested)
289 were achieved through the examination of 1) the percentage of explained variance, 2) the
290 shape of residuals, 3) the split half analysis and 4) the random initialization using the Tucker
291 Congruence Coefficients (Tedetti et al., 2012). The fluorescence intensities of each
292 component found are given in QSU. The fluorescence intensities in QSU provided for each
293 sample is the mean of the two replicates with a coefficient of variance (CV) < 10 %.

294

295 **2.5. Biogeochemical and biological analyses**

296 Filters for the determination of the TChl *a* concentration were collected by filtering 550
297 mL of sample water onto a GF/F filter (Whatman). The filters were directly shock-frozen and
298 stored in liquid N₂. TChl *a* was extracted in methanol and measured by fluorometry (Le
299 Bouteiller et al., 1992). The precision of the measurement was $\pm 0.005 \mu\text{g L}^{-1}$.

300 For the determination of phycoerythrin concentration, water samples (3-4 L) were
301 filtered onto 0.4- μ m Nucleopore polycarbonate filters and immediately frozen in liquid N₂
302 until analysis. Phycoerythrin was extracted in a 4 mL glycerol-phosphate mixture (50/50)
303 according to Neveux et al. (2009) after vigorous shaking for resuspension of particles
304 (Wyman, 1992), and then quantified by fluorometry using a Perkin Elmer LS55
305 spectrofluorometer (λ_{Ex} : 450-580 nm at λ_{Em} of 605 nm) (Lantoine and Neveux, 1997). The
306 measurement precision was ~ 16 %.

307 Pico- and nano-phytoplankton abundances were analyzed by flow cytometry. Samples
308 (1.8 mL) were collected from the mesocosm everyday from 1, 6 and 12 m depth in cryotubes,
309 fixed with 200 μ L of paraformaldehyde (4 % final concentration), left 15 min at ambient
310 temperature, flash frozen in liquid N₂ and stored at -80 °C until analysis on a FACSCalibur
311 (BD Biosciences) flow cytometer as described in Marie et al. (1999). Before analysis, samples
312 were thawed at ambient temperature in the dark. 600 μ L of each sample were mixed and
313 homogenized with 25 μ L of TrueCount beads and 10 μ L of 2 μ m diameter beads
314 (Fluoresbryte™, Polysciences) used as a reference for size discrimination between pico- and
315 nano-phytoplankton. Phytoplankton communities were clustered as *Prochlorococcus* spp. cell
316 like, *Synechococcus* spp. cell like, nanoeukaryotes cell like and picoeukaryotes cell like
317 according to their optical properties (light scattered and fluorescence emission by the cells)
318 (Marie et al., 1999).

319 For the determination of microphytoplankton community composition (diatoms), water
320 samples (250 mL) were taken every day by pumping and preserved with formalin. In the
321 laboratory, samples were sedimented and microphytoplankton species were identified and
322 enumerated under inverted microscope.

323 Bacterial production (BP) was estimated using the ³H-leucine incorporation technique
324 (Kirchman et al., 1985), adapted to the centrifugation method (Smith and Azam, 1992).

325 Radioactivity was counted using a Liquid Scintillation Analyzer Packard 2100 TR and the ^3H
326 counting efficiency was corrected for quenching. BP was calculated from leucine
327 incorporation rates using the conversion factor of $1.5 \text{ kg C mol}^{-1}$ leucine, and is shown here in
328 $\text{ng C L}^{-1} \text{ h}^{-1}$.

329 Samples for total organic carbon (TOC) concentrations were collected in duplicate in
330 precombusted (4 h, $450 \text{ }^\circ\text{C}$), 12-mL sealed glassware flask, acidified with orthophosphoric
331 acid and stored in dark at $4 \text{ }^\circ\text{C}$ until analysis. Samples were analyzed by using a TOC-5000
332 total carbon analyzer (Sohrin and Sempéré, 2005). The average TOC concentrations in the
333 Deep Atlantic Water and low carbon water reference standards were $45 \pm 2 \text{ } \mu\text{M C}$, $n = 24$ and
334 $1 \pm 0.3 \text{ } \mu\text{M C}$, $n = 24$, respectively. The analytical precision of the procedure was $\leq 2 \%$.

335 Dissolved organic nitrogen (DON) concentrations were calculated from total nitrogen
336 (TN) concentrations subtracted by particulate organic nitrogen (PON) and dissolved inorganic
337 nitrogen (DIN) concentrations. Samples were collected in 50 mL glass bottles and stored at
338 $-20 \text{ }^\circ\text{C}$ until analysis. The samples were divided in two parts after a rapid thaw for analysis of
339 both organic and inorganic concentrations. TN concentration was determined according to the
340 wet oxidation procedure described in Pujo-Pay and Raimbault (1994). Samples for PON
341 concentrations were collected by filtering 1 L of water on GF/F filters and analyzed according
342 to the wet oxidation protocol (Pujo-Pay and Raimbault, 1994) with a precision of $0.06 \text{ } \mu\text{M}$.
343 DIN concentration was determined according to Aminot and K  rouel (2007). Measurements
344 were conducted using a segmented flow auto-analyser (AutoAnalyzer AA3 HR, SEAL
345 Analytical).

346

347 **2.6. Statistics**

348 Linear regression analyses and one-way analyses of variance (ANOVA) were
349 performed with StatView 5.0 and the statistics package provided in Microsoft Excel 11.0.

350 ANOVA was used to compare the means of independent data groups (normally distributed).
351 For the different analyses and tests, the significance threshold was set at $p < 0.05$.

352

353 **3. Results**

354

355 **3.1. Evolution of the core parameters in the mesocosm**

356 The detailed description of temperature, salinity and nutrient concentrations in the three
357 mesocosms is provided in Bonnet et al. (2015). Briefly, water temperature progressively
358 increased inside and outside the mesocosms from 25.4 to 26.2 °C over the course of the 23-
359 day experiment. Salinity also progressively increased from 35.1 to 35.5 but this increase was
360 less pronounced in the surrounding waters with salinities of 35.4 at day 23. Temperature and
361 salinity were homogeneous over depth in the mesocosms, the water column having been well
362 mixed throughout the experiment. In the mesocosms, average concentrations of $\text{NO}_3^- + \text{NO}_2^-$
363 were $< 0.04 \mu\text{M}$ before the DIP fertilization (day 4) and decreased to $0.01 \mu\text{M}$ at the end of
364 the experiment. In contrast, NH_4^+ concentrations were $\sim 0.01 \mu\text{M}$ up to day 18, and then
365 increased up to $0.06 \mu\text{M}$ at day 23. DIP concentrations increased from $0.02\text{-}0.05 \mu\text{M}$ before
366 the fertilization to $0.8 \mu\text{M}$ just after, and decreased gradually over time to return to their initial
367 concentrations at day 23 ($0.02\text{-}0.08 \mu\text{M}$). In the surrounding waters, NO_3^- remained < 0.20
368 μM and DIP was $0.05 \mu\text{M}$ all over the experiment (Berthelot et al., 2015; Bonnet et al., 2015).

369 For all the parameters described below, including CDOM and FDOM data, no
370 significant difference was found with depth, except for TChl *a* and PON whose
371 concentrations were higher at 12 m depth than at 1 and 6 m depths (ANOVA, $n = 20\text{-}22$, $p =$
372 $0.003\text{-}0.04$). Therefore, in the following paragraphs, the parameter descriptors are generally
373 given in term of depth-averaged values.

374

375 **3.2. Evolution of phytoplankton biomass, bacterial production and organic**
376 **N and C pools in the mesocosm**

377 TChl *a*, PON concentrations and BP in the mesocosm M1 and in the surrounding waters
378 (OUT) generally increased throughout the experiment, with a decrease from day 4 to day 9
379 and then an increase from day 9 to the end of the experiment (Fig. 3a,d,f). This increase was
380 more pronounced in M1, where TChl *a*, PON concentrations and BP varying from 0.12 to
381 0.55 $\mu\text{g L}^{-1}$, 0.65 to 1.31 μM and 85 to 681 $\text{ng C L}^{-1} \text{h}^{-1}$, respectively. TChl *a*, PON
382 concentrations and BP were significantly higher inside M1 during P2 (day 15 to day 23) than
383 inside M1 during P1 (day 5 to day 14), and than outside during P1 and P2 (ANOVA, $n = 25-$
384 30, $p < 0.0001-0.004$) (Table 1). Phycoerythrin concentration decreased from day 4 (0.36 μg
385 L^{-1}) to day 9 (0.05 $\mu\text{g L}^{-1}$), increased towards day 16 (0.34 $\mu\text{g L}^{-1}$) and then oscillated to
386 return to the value of 0.34 $\mu\text{g L}^{-1}$ at day 23 (Fig. 3b). In contrast, in OUT, phycoerythrin
387 concentration increased from day 9 to the end of the experiment, showing a strong raise at day
388 21 (0.85 $\mu\text{g L}^{-1}$). Thus, during P2, phycoerythrin concentration was significantly higher
389 outside M1 than inside (ANOVA, $n = 9$, $p = 0.004$) (Table 1). The TOC concentration
390 decreased from day 4 (70 μM) to day 11 (64 μM) and increased from day 11 to day 22 (81
391 μM) (Fig. 3c). This increase in the second part of the experiment was not observed in OUT.
392 Although the TOC concentration was significantly higher during P2 than during P1 in M1
393 (ANOVA, $n = 9$, $p = 0.03$), there was no difference between M1 and OUT during P2
394 (ANOVA, $n = 7-9$, $p = 0.2$) (Table 1). The DON concentration was rather constant and only
395 tended to decrease during P2 (Fig. 3e). No significant difference in DON concentrations was
396 found between M1 and OUT (ANOVA, $n = 22-29$, $p = 0.07-0.7$) (Table 1).

397 The abundance of diazotrophs DDAs inside M1 increased from day 3 (77×10^3 *nifH*
398 copies L^{-1}) to day 9 (190×10^3 *nifH* copies L^{-1}), decreased from day 9 to day 15 (5.4×10^3
399 *nifH* copies L^{-1}) and finally increased from day 15 to day 23 (78×10^3 *nifH* copies L^{-1}). In

400 OUT a quite similar pattern was observed despite a high value of 450×10^3 *nifH* copies L⁻¹ at
401 day 18 (Fig. 4a). No significant difference in the abundance of DDAs was observed in M1
402 between P1 and P2, and between M1 and OUT (ANOVA, $n = 3-6$, $p = 0.05-0.8$) (Table 1). On
403 the other hand, the abundance of diazotrophic Group UCYN-C strongly increased from day 9
404 (0.54×10^3 *nifH* copies L⁻¹) to day 23 (110×10^3 *nifH* copies L⁻¹) in M1, while it increased
405 much more slowly in OUT from day 10 (0.32×10^3 *nifH* copies L⁻¹) to day 22 (4.8×10^3 *nifH*
406 copies L⁻¹) (Fig. 4b). Hence, the abundance of UCYN-C was much higher in M1 during P2
407 than in M1 during P1 (14 times higher) and than in OUT during P1 and P2 (22-53 times
408 higher) (ANOVA, $n = 3-6$, $p < 0.0001$) (Table 1). It should be noticed that the abundances of
409 DDAs and UCYN-C are reported as *nifH* (gene) copies L⁻¹ rather than cells L⁻¹ because there
410 is currently little information about the number of *nifH* copies per genome in these diazotroph
411 targets (Turk-Kubo et al., 2015). Total diatoms in M1 decreased from day 2 (47×10^3 cell L⁻¹)
412 to day 9 (6×10^3 cell L⁻¹) and then oscillated to reach 41×10^3 cell L⁻¹ at the end of the
413 experiment, with a maximum value of 120×10^3 cell L⁻¹ at day 15 (Fig. 4c). This was
414 essentially due to the large diatom *Cylindrotheca closterium* (data not shown). No difference
415 in abundance of total diatoms was observed between P1 and P2 (ANOVA, $n = 5$, $p = 0.2$).
416 The abundances of *Synechococcus* spp., *Prochlorococcus* spp., picoeukaryotes and
417 nanoeukaryotes decreased from day 4 (~ 43, 16, 2.2 and 0.9×10^3 cell mL⁻¹, respectively) to
418 day 9 (~ 18, 5, 0.8 and 0.6×10^3 cell mL⁻¹, respectively) (Fig. 4d-g). From day 9 to the end of
419 the experiment, the abundance of *Synechococcus* spp. and picoeukaryotes noticeably
420 increased to reach ~ 90 and 3.4×10^3 cell mL⁻¹ at day 23 respectively, whereas the increase in
421 *Prochlorococcus* spp. and nanoeukaryotes was much less (to ~ 20 and 1.3×10^3 cell mL⁻¹ at
422 day 23, respectively). The abundance of *Synechococcus* spp., picoeukaryotes and
423 nanoeukaryotes was significantly higher in P2 than in P1 (ANOVA, $n = 23-24$, $p < 0.0001$ -

424 0.002), while that of *Prochlorococcus* spp. was not different (ANOVA, $n = 23-24$, $p = 0.07$)
425 (Table 1).

426

427 **3.3. Absorption spectra of CDOM and particulate matter**

428 CDOM absorption spectra of samples collected in M1 and OUT were quite similar,
429 displaying an exponential decrease in $a_g(\lambda)$ without any significant shoulder (Fig. 5). $a_p(\lambda)$
430 spectra, which reflect the absorption by both phytoplankton and NAP, were characterized by
431 two main Chl *a* peaks, one between 432 and 442 nm (at 436 nm on average) and one between
432 672 and 682 nm (at 676 nm on average), while several shoulders also emerged at 376, 416,
433 464, 490 and 550 nm (Fig. 5). Hereafter, $a_g(\lambda)$ is presented at 370 and 442 nm, while $a_p(\lambda)$ is
434 given at 442 and 676 nm, the two latter wavelengths corresponding to the absorption maxima
435 of Chl *a*.

436

437 **3.4. Evolution of absorption coefficients, spectral slope in the mesocosm**

438 In M1, absorption coefficients decreased from day 4 to day 9 and then increased from
439 day 9 to the end of the experiment (day 23), leading to variations in the ranges 0.041-0.067 m⁻¹
440 ¹ for $a_g(370)$, 0.011-0.020 m⁻¹ for $a_g(442)$, 0.009-0.025 m⁻¹ for $a_p(442)$ and 0.003-0.012 m⁻¹
441 for $a_p(676)$ (Fig. 6a,b,d,e). In OUT, these parameters also increased from day 9 or 10 to day
442 23 but with lower amplitude. Inside M1, all these absorption coefficients were significantly
443 higher during P2 than during P1 (ANOVA, $n = 27-30$, $p < 0.0001$). However, only $a_g(370)$
444 and $a_p(442)$ were significantly higher in M1 than outside during P2 (ANOVA, $n = 9-27$, $p =$
445 0.004-0.02) (Table 1). S_g inside and outside M1, ranging from 0.0148 to 0.0188 nm⁻¹, did not
446 display any clear pattern throughout the experiment (Fig. 6c).

447

448 **3.5. Spectral characteristics and identification of FDOM components**

449 Three FDOM components (C1-C3) were identified by the PARAFAC model validated
450 on 130 EEM samples from M1 and OUT. The spectral characteristics of C1-C3 are reported
451 in Fig. 7. These components exhibited one or two Ex maxima and one Em maximum. C1,
452 with a maximum at $\lambda_{Ex}/\lambda_{Em}$ of 230/476 nm, corresponded to the category of UVC humic-like
453 fluorophores, referred to as peak A (Coble, 1996; 2007; Ishii and Boyer, 2012). C2 and C3
454 had two maxima each, located at $\lambda_{Ex1}, \lambda_{Ex2}/\lambda_{Em}$ of 225, 280/344 nm and 225, 275/304 nm,
455 respectively (Fig. 7). They belonged to the group of protein-like fluorophores, C2 being
456 analogous to tryptophan-like fluorophore (peaks T) and C3 being analogous to tyrosine-like
457 fluorophore (peaks B) (Coble, 1996; 2007).

458

459 **3.6. Evolution of FDOM components in the mesocosm M1**

460 Inside M1, the fluorescence intensity of humic-like fluorophore decreased from day 2 (~
461 5.3 QSU) to day 8 (~ 2.7 QSU), increased from day 8 to day 14 (~ 4.8 QSU) and dropped
462 down to ~ 2.5 QSU at day 15. Then, it increased to reach ~ 5.6 QSU at day 20 (Fig. 8a). The
463 fluorescence intensity of tryptophan-like fluorophore decreased from day 3 (~ 9.1 QSU) to
464 day 8 (~ 5.3 QSU) (Fig. 8b). At day 9, it increased up to ~ 8.3 QSU and remained relatively
465 stable up to day 14 (~ 8.4 QSU). After a reduction at day 15 (~ 5.9 QSU), the fluorescence
466 intensity increased up to the end of the experiment (~ 10.4 QSU at day 20). The fluorescence
467 intensity of tyrosine-like fluorophore decreased from day 5 (~ 8.2 QSU) to day 15 (~ 3.9
468 QSU) and then slowly increased to day 20 (~ 6.2 QSU) (Fig. 8c). While for humic- and
469 tryptophan-like fluorophores no differences in their fluorescence intensity were observed
470 between P1 and P2 (ANOVA, $n = 18-30$, $p = 0.4-0.9$), the fluorescence intensity of tyrosine-
471 like fluorophore was significantly lower during P2 (ANOVA, $n = 18-28$, $p = 0.002$) (Table 1).
472 Overall, the FDOM pool was dominated by protein-like material: the combined fluorescence

473 of tryptophan and tyrosine fluorophores ranged from 9.1 to 22.3 QSU, while the fluorescence
474 of humic fluorophore ranged from 1.9 to 6.2 QSU.

475

476 **3.7. Relationships between the chromophoric and the** 477 **biogeochemical/biological parameters**

478 Table 2 presents r values of linear regressions between the chromophoric and the
479 biogeochemical/biological parameters for the samples collected in M1 from day 5 to day 20.
480 Here we consider that only the correlations that are very highly significant ($p < 0.0001$) reflect
481 relevant linear relationships. $a_g(370, 442)$ and $a_p(442, 676)$ were not that much correlated to
482 each other ($r = 0.52-0.62$, $n = 36$, $p < 0.0001-0.002$). S_g was not correlated to $a_g(370, 442)$ ($r =$
483 $0.15-0.22$, $n = 36$, $p = 0.06-0.9$). Even though humic- and tryptophan-like fluorophores were
484 very highly correlated ($r = 0.67$, $n = 36$, $p < 0.0001$), they did not show any coupling with
485 tyrosine-like fluorophore ($r = 0.20-0.48$, $n = 36$, $p = 0.005-0.2$). Moreover, none of these three
486 fluorophores was very highly correlated to the absorption coefficients and spectral slope ($r =$
487 $0.09-0.42$, $n = 36$, $p > 0.5-0.05$) (Table 2). These correlations emphasize the decoupling
488 between the CDOM and FDOM materials during the experiment.

489 All absorption coefficients were very highly positively correlated to *Synechococcus* spp.
490 abundance ($r = 0.76-0.83$), BP ($r = 0.72-0.78$), TChl a concentration ($r = 0.60-0.88$), PON
491 concentration ($r = 0.58-0.75$) and picoeukaryote abundance ($r = 0.52-0.71$) ($n = 36$, $p <$
492 0.0001). Linear relationships between $a_g(370)$ or $a_p(442)$ and *Synechococcus* spp. abundance
493 are presented in Fig. 9. S_g as well as the three FDOM fluorophores did not present any highly
494 significant correlation with the biogeochemical/biological constituents. Phycoerythrin, TOC,
495 DDAs, UCYN-C and total diatoms did not display any very highly significant correlations
496 with the chromophoric parameters although some r values were quite high [for instance 0.90
497 between UCYN-C and $a_p(442)$]. This is because these correlations were determined for a

498 lower number of samples (8-15). Nonetheless, albeit not very highly significant, these
499 relationships highlighted interesting trends such as positive (negative) relationships between
500 absorption coefficients (tyrosine-like fluorophore) and UCYN-C abundance, and negative
501 (positive) relationships between absorption coefficients (tyrosine-like fluorophore) and DDA
502 abundance (Table 2).

503

504 **4. Discussion**

505

506 **4.1. General characteristics of chromophoric material**

507 *CDOM absorption.* CDOM absorption spectra from samples inside and outside the
508 mesocosm did not display any significant shoulder in the range 370-720 nm (Fig. 5). In the
509 same way, using the PSICAM, Röttgers and Koch (2012) did not observe any specific feature
510 in the CDOM absorption spectra from 380 to 700 nm of samples collected in the surface
511 waters of the tropical Atlantic Ocean and of the North East and South West Pacific, including
512 our study area inside the barrier reef of New Caledonia.

513 $a_g(370)$ and $a_g(442)$ measured inside and outside the mesocosm (0.040-0.086 and 0.011-
514 0.022 m^{-1} , respectively; Fig. 6a,b) were within the range of those measured in surface waters
515 of the Atlantic Ocean and at 80-200 m depth in the South West Pacific (offshore of New
516 Caledonia) (0.021-0.118 and 0.004-0.039 m^{-1} , respectively) (Röttgers and Doerffer, 2007;
517 Röttgers and Koch, 2012; Dupouy et al., 2014). In addition, our $a_g(370)$ and $a_g(442)$ values
518 were slightly lower than those measured in the subtropical North Pacific and the
519 Mediterranean Sea (0.050-0.090 and 0.018-0.035 m^{-1} , respectively) (Yamashita et al., 2013;
520 Organelli et al., 2014) but higher than those observed in the center of the gyre of the South
521 East Pacific (> 0.010 -0.035 and 0.005-0.015 m^{-1} , respectively) (Bricaud et al., 2010).

522 Our S_g values determined over the range 370-500 nm varied between 0.015 and 0.019
523 nm^{-1} inside and outside the mesocosm (Fig. 6c). They were to some extent lower than S_g
524 values determined between 350 and 500 nm of surface waters of the Mediterranean Sea,
525 Atlantic Ocean and South East Pacific (0.015-0.025 nm^{-1}) (Röttgers and Doerffer, 2007;
526 Bricaud et al., 2010; Para et al., 2010; Organelli et al., 2014). In fact, our S_g values did not
527 reach the maximal values encountered in oligotrophic areas (0.020-0.025 nm^{-1}) despite the
528 potentially important CDOM photobleaching processes which would have occurred in the
529 surface waters of the mesocosm. This is explained by the different spectral ranges used for the
530 S_g determination (370-500 nm vs 350-500 nm). Indeed, S_g , which strongly depends on the
531 chosen wavelength interval, is generally higher for intervals in the short wavelengths (Nelson
532 and Siegel, 2013; Sempéré et al., 2015), and do not present a constant spectral slope but rather
533 steeper slopes towards the short UV wavelengths (Tedetti et al., 2007; Sempéré et al., 2015).
534 Hence, this difference of 20 nm in the wavelength interval may influence the S_g values, the
535 latter decreasing when considering the range 370-500 nm. It is worth noting that no
536 correlation was found between $a_g(370)$ or $a_g(442)$ and S_g (Table 2). This was probably
537 attributable to the low ranges and the low values of both $a_g(\lambda)$ and S_g reported here.

538 ***FDOM.*** The three FDOM components identified in this work were UVC humic-,
539 tryptophan- and tyrosine-like fluorophores (Fig. 7). Thus, FDOM was dominated by protein-
540 like material, i.e. compounds containing nitrogen, while humic-like material was less
541 represented. Of these protein-like compounds, tryptophan- and tyrosine-like fluorophores
542 have been reported in many aquatic ecosystems (see reviews by Coble, 2007; Fellman et al.,
543 2010). They represent compounds of low molecular weight at the state of free amino acids or
544 amino acids bound in peptides or proteins. They are known to be released by autochthonous
545 (marine) phytoplankton activity and serve as fresh and labile bioavailable products for
546 heterotrophic bacteria (Yamashita and Tanoue, 2004; Nieto-Cid et al., 2006; Davis and

547 Benner, 2007; Romera-Castillo et al., 2010; Tedetti et al., 2012). Moreover, they can be
548 directly associated to humic substances (Stedmon and Cory, 2014). Generally, they do not
549 show any conservative behaviour in the salinity gradient (Kowalczuk et al., 2009). UVC
550 humic-like fluorophore (“peak A”) corresponds to component 1 ($\lambda_{EX}/\lambda_{EM}$: < 230-260/400-500
551 nm) in the review paper by Ishii and Boyer (2012) and is one of the most widespread humic-
552 like components in the aquatic environment (Kowalczuk et al., 2009; 2013). This fluorophore,
553 which absorbs light at very short wavelengths (230 nm) and fluoresce in long visible
554 wavelengths (476 nm) resulting in a high Stokes shift (246 nm), would be of relatively low
555 molecular weight (< 1 kDa) compared to other fluorescent humic-like materials (Ishii and
556 Boyer, 2012). Present in higher quantities in the photic zone and shallow surface waters, this
557 humic-like component is recognized as a photodegradation product of marine organic matter
558 (Yamashita et al., 2008; Ishii and Boyer, 2012) and appears to be resistant to biodegradation
559 (Balcarczyk et al., 2009; Fellman et al., 2010; Lønborg et al., 2015).

560 ***Particulate absorption.*** Particulate absorption coefficient spectra were dominated by
561 phytoplankton absorption [$a_p(\lambda)$] with the presence of the two main peaks of Chl *a* (at 436 and
562 672 nm), whereas the influence of detrital material (NAP), characterized by an exponential
563 decrease of absorption with wavelength, was not really visible upon these spectra (Fig. 5).
564 Besides these two main peaks, several shoulders were found between 376 and 550 nm.
565 Actually, the shoulders at 376 and 416 nm might be related to Chl *a* (Stuart et al., 1998;
566 Lohrenz et al., 2003). The shoulders at 464 and 490 nm reflected the occurrence of
567 photosynthetic carotenoids and/or non photosynthetic (photoprotective) carotenoids (Dupouy
568 et al., 1997; 2003; Stuart et al., 1998; Wozniak et al., 1999; Lohrenz et al., 2003; Bricaud et
569 al., 2004). In addition, the shoulder at 490 nm may be related to the presence of phycourobilin
570 (PUB). PUB, which absorbs light around 490 nm, is known to be contained in phycoerythrin
571 of cyanobacteria, such as *Synechococcus* spp., living in the open ocean. PUB is indeed

572 considered as a chromatic adaptation to blue radiation which penetrates deeper than other
573 wavelengths in the water column (Neveux et al., 1999). Also, the small shoulder at 550 nm
574 could be the sign of phycoerythrobilin (PEB), also contained in phycoerythrin. PEB,
575 absorbing light around 550-565 nm, is present in higher amount in *Synechococcus* spp. of
576 coastal environments (Neveux et al., 1999). Pronounced shoulders or peaks at 550 nm are
577 observed only for exceptional *Synechococcus* spp. concentrations ($> 3 \times 10^5$ cell mL⁻¹) with
578 TChl *a* $> 1 \mu\text{g L}^{-1}$ (Morel, 1997) or more commonly for large filamentous cyanobacteria in
579 tropical waters (Dupouy et al., 2008). An attribution of the shoulders at 490 and 550 nm to
580 PUB and PEB, respectively appears reasonable regarding the fact that PUB and PEB signals
581 were detected in the phycoerythrin fluorescence measurements (M. Rodier, pers. comm.).
582 Such a proportion of *Prochlorococcus* spp. and *Synechococcus* spp. counts reported in this
583 work are typical of the New Caledonia lagoon (Neveux et al., 2009) compared to the
584 equatorial upwelling area where this is inversed (Dupouy et al., 2003).

585 Absorption coefficients of particulate matter at 442 and 676 nm [$a_p(442)$ and $a_p(676)$]
586 measured inside and outside the mesocosm at the exit of the New Caledonian coral lagoon
587 (0.006-0.031 and 0.0013-0.013 m⁻¹, respectively; Fig. 6d,e) were slightly lower than those
588 measured with the same instrument in the surface waters within the New Caledonian lagoon
589 (0.008-0.040 and 0.0030-0.018 m⁻¹, respectively) (Röttgers et al., 2014; Dupouy et al., 2014),
590 the latter values being linked to an exceptional increase in total phytoplankton biomass during
591 the 2008 Valhybio cruise in response to a *La Nina* heavy rain episode (Dupouy et al., 2009;
592 Fuchs et al., 2012).

593

594 **4.2. Coupling between the dynamics of chromophoric material and that of**
595 **N₂ fixation in the mesocosm**

596 ***Link between absorption and Synechococcus spp.*** Several observations suggest the
597 observed change in particulate matter absorption [$a_p(\lambda)$] during the experiment was mainly
598 driven by *Synechococcus* spp. Several observations may support this hypothesis. Firstly,
599 *Synechococcus* spp. was the most abundant group among (non-diazotrophic) pico-, nano- and
600 micro-phytoplankton communities in the mesocosm (Fig. 4c-g). For instance, the
601 concentration of *Synechococcus* spp. ($88 \pm 14 \times 10^3$ cell mL⁻¹ in P2) was higher by a factor ~
602 1000 relative to that of total diatoms ($44 \pm 37 \times 10^3$ cell L⁻¹ in P2) (Table 1). *Synechococcus*
603 spp. abundance cannot in first approach be compared to those of diazotrophs (given in *nifH*
604 copies L⁻¹). However, assuming that there was a minimum of one *nifH* gene copy per cell, the
605 number of *nifH* (gene) copies L⁻¹ may reflect the upper limit of the number of cells L⁻¹, though
606 DNA and RNA extractions were probably < 100% (Foster et al., 2009). In this sense, the
607 concentration of *Synechococcus* spp. was higher by a factor ~ 1000 relative to that of UCYN-
608 C ($64 \pm 24 \times 10^3$ *nifH* copies L⁻¹, given a maximum of $64 \pm 24 \times 10^3$ cell L⁻¹ in P2) (Table 1).
609 Thus, we conclude that *Synechococcus* spp. was very likely the most important group among
610 non-diazotrophic and diazotrophic communities in the mesocosm. Secondly, *Synechococcus*
611 spp. is known to have significant absorption properties in the visible domain, highlighted in
612 culture experiments (Bidigare et al., 1989; Morel et al., 1993; Stramski and Mobley, 1997;
613 Lutz et al., 2001) but also in natural samples (Morel, 1997). Absorption properties of
614 *Synechococcus* spp. have been compared to those of *Prochlorococcus* spp. and
615 nanoplanktonic diatoms. The efficiency factor for absorption (given for a cell), which depends
616 on both the size and the internal pigment concentration, was on average two times higher for
617 *Prochlorococcus* spp. and three times higher for nanoplanktonic diatoms than for
618 *Synechococcus* spp. over the visible domain (Morel et al., 1993; Stramski and Mobley, 1997).
619 Considering than the number of cells of *Synechococcus* spp. was on average 6 times higher
620 than that of *Prochlorococcus* spp. and ~ 1000 times higher than that of total diatoms during

621 P2, we may put forward that *Synechococcus* spp was the main contributor to visible
622 absorption in the mesocosm. Finally, $a_p(442)$ and $a_p(676)$ showed the highest positive
623 correlation with *Synechococcus* spp. abundance (Table 2; Fig. 9) with a very similar evolution
624 during P1 and P2 (Fig. 4d, 6d,e).

625 The absorption of CDOM also presented the highest (positive) coupling with
626 *Synechococcus* spp. abundance and BP (Fig. 3f, 4d, 6a,b; Table 2; Fig. 9), thereby suggesting
627 CDOM was produced by heterotrophic bacteria from their assimilation of labile organic
628 compounds released by *Synechococcus* spp. Indeed, the latter has been shown to release
629 DOM (Bronk, 1999; Becker et al., 2014) that may be directly used to support heterotrophic
630 activity (Nagata, 2000; Lefort and Gasol, 2014). These (non-colored) labile organic substrates
631 issued from *Synechococcus* spp. would be converted into chromophoric, more refractory
632 compounds by heterotrophic bacteria (Nelson et al., 1998; Rochelle-Newall and Fisher, 2002;
633 Nelson and Siegel, 2013). Currently, the coupling between phytoplankton and heterotrophic
634 bacteria seems to be recognized as a major pathway for the formation of CDOM in the ocean
635 (Rochelle-Newall and Fisher, 2002; Nelson and Siegel, 2013; Organelli et al., 2014).
636 Interestingly, Biers et al. (2007) highlighted the role of DON, specifically amino sugars and
637 aromatic amino acids, in the microbial production of CDOM and FDOM while Bronk et al.
638 (1999) reported the production of DON by *Synechococcus* spp. Consequently, the works by
639 Biers et al. (2007) and Bronk et al. (1999) support the assumption of the CDOM production
640 by heterotrophic bacteria consecutive to their utilization of labile DOM (that would be in part
641 in the form of DON) released by *Synechococcus* spp. cyanobacteria. CDOM could be also
642 produced directly from *Synechococcus* spp., as mentioned by Romera-Castillo et al. (2011).
643 Also, we cannot exclude the participation of other primary producers, such as diatoms, to the
644 CDOM production through a direct release of colored material (Romera-Castillo et al., 2010;
645 Chari et al., 2013) or through the bacterial re-working. For example, from culture

646 experiments, Chari et al. (2013) reported the production of CDOM by *Cylindrotheca*
647 *closterium*, one of the most important diatom species in the mesocosm. Regarding the
648 respective abundances of *Synechococcus* spp. and diatoms and their evolution all over the
649 experiment, it seems however that *Synechococcus* spp. was a greater contributor to CDOM
650 than diatoms. Consequently, even though it seems difficult here to discriminate the respective
651 contributions of cyanobacterial primary producers (*Synechococcus* spp.) and heterotrophic
652 bacteria in the production of CDOM, unambiguously the coupling between both plays a key
653 role in the absorption of particulate and dissolved chromophoric material in the mesocosm.

654 ***Link between absorption, Synechococcus spp. and N₂ fixation.*** During the first part of
655 the experiment (P1), the diazotrophic community was dominated by diatoms-diazotrophs
656 associations (DDAs) (Fig. 4a), more specifically heterocyst-forming *Richelia* associated with
657 *Rhizosolenia* (Turk-Kubo et al., 2015). The decrease observed in phytoplankton biomass
658 (including diatoms, *Synechococcus* spp., *Prochlorococcus* spp., pico- and nano-eukaryotes),
659 BP and organic C/N pools from day 4 to day 9-11 (Fig. 3a-d,f; Fig. 4c-g) was attributable to a
660 N limitation. In fact, during the first days, phytoplankton would have consumed the small
661 stock of nitrates remaining in the water column without new inputs. In addition, DDAs would
662 not have been a significant source of N for its surrounding environment because *Richelia*
663 would have given the major part of the N that they had fixed to their host diatoms (Berthelot
664 et al., 2015). This decrease in *Synechococcus* spp. and BP led to the decrease in CDOM and
665 particulate matter absorption (Fig. 6a,b,d,e). During P1, the total amount of N issued from the
666 N₂ fixation was equivalent to the total amount of PON exported, suggesting there is a rapid
667 and possibly direct export of the recently fixed N₂ by DDAs (Berthelot et al., 2015). In the
668 second part of the experiment (P2), unicellular cyanobacteria Group C (UCYN-C) became the
669 dominant diazotrophs (Fig. 4b). The UCYN-C bloom was induced by the phosphate
670 fertilization and increasing temperatures (Turk-Kubo et al., 2015). Consequently, N₂ fixation

671 rates were higher during P2 than during P1 (Berthelot et al., 2015). From these authors, the N
672 released by UCYN-C (in the form of DON and/or NH_4^+) allowed for supporting non-
673 diazotrophic cyanobacterial and heterotrophic bacterial growths. This would have in turn
674 stimulated the production of dissolved and particulate chromophoric materials [increase in
675 TChl *a*, PON, TOC, BP, *Synechococcus* spp., $a_g(370, 442)$ and $a_p(442, 676)$ from day 9-11 to
676 day 21-23; Fig. 3a,c,d,f; Fig. 4d; Fig. 6a,b,d,e]. The enhancement of *Synechococcus* spp. *via*
677 the release of N by diazotrophs has been already underscored by Agawin et al. (2007). This N
678 release could also explain the strong increase in diatoms (mainly *Cylindrotheca closterium*) at
679 day 15 (Fig. 4c). In P2, both N_2 fixation and DON consumption were significant N sources
680 for primary production and might explain the PON production (Berthelot et al., 2015). It is
681 worth noting that a perfect temporal synchronization occurred between the variations of
682 *Synechococcus* spp./BP and the variations of CDOM and particulate matter absorption. This
683 implies rapidity in the production mechanisms of the chromophoric material inside the
684 mesocosm. The variations of S_g (Fig. 6c) [no correlation with $a_g(370, 442)$; Table 2]
685 suggested that CDOM absorption was not only influenced by production processes but was
686 also probably affected by photo- and microbial-degradation processes. It is very likely that
687 these degradation processes were not intense enough to counterbalance the production of
688 CDOM by the couple *Synechococcus* spp./heterotrophic bacteria.

689 **Absorption budget.** Also, the contribution of CDOM (a_g) to the total absorption (a_{g+p})
690 remained high in the UV domain (370 nm), ranging from 72 to 96 %, while it decreased from
691 the beginning (50-66 %) to the end of the experiment (40-48 %) in the visible domain (442
692 nm). These percentages in the UV and visible domains are in line with those reported in the
693 literature for the open ocean (Siegel et al., 2002; 2005; Tedetti et al., 2010), the higher
694 contribution of particulate material in the absorption budget at 442 nm during the second part

695 of the experiment being explained by the bloom of cyanobacterial primary producers
696 (*Synechococcus* spp.).

697 ***FDOM decoupling.*** FDOM did neither follow the evolution of CDOM nor the
698 evolution of heterotrophic bacteria and *Synechococcus* spp. (Fig. 8; Table 2). The evolution of
699 tyrosine-like fluorophore, whose fluorescence intensity was higher in P1 than in P2 (Table 1),
700 tended to be close to that of DDAs (Fig. 4a, 8c; Table 2). Therefore, we may hypothesize a
701 role of these diatoms-diazotrophs associations in the production of the tyrosine-like material.
702 The tyrosine-like fluorophore released by phytoplankton could then be consumed by
703 heterotrophic bacteria as labile substrates. UVC humic-like fluorophore displayed an
704 evolution close to that of tryptophan material with two important decreases at days 7-8 and
705 15. This observation supports the hypothesis by Stedmon and Cory (2014) of an association
706 between humic substances and tryptophan fluorophore in seawater. This revealed that the
707 humic-like component was also subjected to production/degradation processes in the
708 mesocosm that cannot be precisely identified here. The fact that CDOM which absorbs light
709 at 370 nm was not fluorescent (no fluorophores with Ex peak at 370 nm) strengthened the
710 assumption that $a_g(370)$ and the three fluorophores represented independent chromophoric
711 materials that were driven by different processes. Also, these fluorophores could be not major
712 components of the CDOM. Consequently, they would absorb but not strongly enough to
713 significantly affect the CDOM variability. Tryptophan- and tyrosine-like fluorophores
714 belonged to the DON pool. Nonetheless, they showed different patterns in the mesocosm:
715 while DON decreased during P2 (both the DON consumption and the N₂ fixation supported
716 the PON production during P2; Berthelot et al., 2015), the two fluorophores tended to
717 increase. This suggested that tryptophan- and tyrosine-like materials were probably not
718 involved in the PON production.

719

720 **5. Conclusion**

721

722 Studies dealing with the CDOM dynamics in the frame of mesocosm experiments
723 remain limited so far and have been conducted merely in coastal-temperate or polar
724 ecosystems (Rochelle-Newall et al., 1999; 2004; Pavlov et al., 2014). This work highlights the
725 spectral characteristics and the variability of dissolved and particulate chromophoric materials
726 throughout a 23-day mesocosm experiment in a tropical, oligotrophic LNLC ecosystem in
727 which N₂ fixers and picophytoplankton play an essential role. Although CDOM did not
728 display any specific shoulders in its absorption spectra, those of particulate chromophoric
729 material were dominated by Chl *a* fingerprint with small signatures of carotenoids,
730 phycourobilin and phycoerythrobilin, which could be related to *Synechococcus* spp., the most
731 abundant cyanobacterial group in the mesocosm. The dynamics of CDOM and particulate
732 matter were strongly coupled with those of *Synechococcus* spp. and bacterial production.
733 Indeed, in the second part of the experiment, the N released in the surrounding environment,
734 very likely by UCYN-C diazotrophs, allowed for supporting cyanobacterial and heterotrophic
735 bacterial growths and subsequently stimulating the production of dissolved and particulate
736 chromophoric materials. The increase in phytoplankton biomass during the second part of the
737 experiment led to a higher contribution of particulate material in the absorption budget at 442
738 nm. FDOM, composed by (N-containing) protein-like fluorophores and UVC humic-like
739 (photoproduct) fluorophore, did not follow the evolution of CDOM and particulate matter,
740 and was thus subjected to different production/degradation processes in the mesocosm.
741 Finally, this study strongly supports the idea of an indirect link between the dynamics of the
742 N₂ fixation and that of chromophoric material in the South West Pacific.

743

744 **Acknowledgements.** Funding for this research was provided by the Agence
745 Nationale de la Recherche (ANR starting grant VAHINE ANR-13-JS06-0002), INSU-LEFE-
746 CYBER program, GOPS, IRD and M.I.O. The authors thank the captain and crew of the R/V
747 *Alis*. We acknowledge the SEOH divers service from the IRD research center of Noumea (E.
748 Folcher, B. Bourgeois and A. Renaud) and from the Observatoire Océanologique de
749 Villefranche-sur-mer (OOV, J.M. Grisoni) as well as the technical service of the IRD research
750 center of Noumea for their helpful technical support. C. Guieu, F. Louis and J.M. Grisoni
751 from OOV are warmly thanked for the mesocosms design and their useful advice for
752 deployment. We also thank A. Desnues, B. Charrière, H. Berthelot, J. Héliou and T. Moutin
753 for their help and assistance in the sampling and analyses. S. Bonnet, PI of the VAHINE
754 project, and J. Neveux are greatly acknowledged for their constructive comments and
755 discussions on the early versions of the manuscript. Two anonymous Reviewers are
756 acknowledged for their relevant comments and corrections, which contributed to improve the
757 quality of this manuscript.

758

759 **References**

- 760 Agawin, N. S. R., Rabouille, S., Veldhuis, M. J. W., Servatius, L., Hol, S., van Overzee, H.
761 M. J., et al. : Competition and facilitation between unicellular nitrogen-fixing
762 cyanobacteria and non-nitrogen-fixing phytoplankton species, *Limnol. Oceanogr.* 52,
763 2233–2248, 2007.
- 764 Aminot, A., and K erouel, R.: Dosage automatique des nutriments dans les eaux marines :
765 m ethodes en flux continu. Ed. Ifremer, M ethodes d’analyse en milieu marin 188 p., 2007.
- 766 Andrew, A. A., Del Vecchio, R., Subramaniam, A., and Blough, N. V.: Chromophoric
767 dissolved organic matter (CDOM) in the Equatorial Atlantic Ocean: Optical properties and
768 their relation to CDOM structure and source, *Mar. Chem.*, 148, 33–43, 2013.
- 769 Antoine, D., Babin, M., Berthon, J. F., Bricaud, A., Gentili, B., Loisel, H., Maritorena, S., and
770 Stramski, D.: Shedding Light on the Sea: Andr e Morel’s Legacy to Optical Oceanography,
771 *Ann. Rev. Mar. Sci.*, 6, 15.1–15.21, 2014.
- 772 Babin, M., Stramski, D., Ferrari, G. M., Claustre, H., Bricaud, A., Obolensky, G., and
773 Hoepffner, N.: Variations in the light absorption coefficients of phytoplankton, nonalgal
774 particles, and dissolved organic matter in coastal waters around Europe, *J. Geophys. Res.*,
775 108(C7), 3211, doi:10.1029/2001JC000882, 2003.
- 776 Balcarczyk, K. L., Jones, J. B. Jr, Jaffe, R., and Maie, N.: Stream dissolved organic matter
777 bioavailability and composition in watersheds underlain with discontinuous permafrost,
778 *Biogeochemistry*, 94, 255–270, 2009.
- 779 Becker, J. W., Berube, P. M. Follett, C. L., Waterbury, J. B., Chisholm, S. W., Delong, E. F.,
780 and Repeta, D. J., 2014. Closely related phytoplankton species produce similar suites of
781 dissolved organic matter, *Front. Microbiol.*, 5, 111, 2014.
- 782 Berthelot, H., Moutin, T., L’Helguen, S., Leblanc, K., H elias, S., Grosso, O., Leblond, N.,
783 Charri ere B., and Bonnet S.: Dinitrogen fixation and dissolved organic nitrogen fueled

784 primary production and particulate export during the VAHINE mesocosms experiment
785 (New Caledonia lagoon), *Biogeosciences*, 12, 4273–4313, 2015.

786 Bidigare, R., Schofield, O., and Prezelin, B.: Influence of zeaxanthin on quantum yield of
787 photosynthesis of *Synechococcus* clone WH 7803 (CD2), *Mar. Ecol. Prog. Ser.*, 56, 177–
788 188, 1989.

789 Biegala, I. C., and Raimbault, P.: High abundance of diazotrophic picocyanobacteria (< 3 µm)
790 in a Southwest Pacific coral lagoon, *Aquat. Microb. Ecol.*, 51, 45–53, 2008.

791 Biers, E. J., Zepp, R. G., Moran, M. A.: The role of nitrogen in chromophoric and fluorescent
792 dissolved organic matter formation, *Mar. Chem.*, 103, 46–60, 2007.

793 Blough, N. V., and Del Vecchio, R.: Chromophoric DOM in the coastal environment. In:
794 Hansel, D.A., Carlson, C.A. (Eds.), *Biogeochemistry of Marine Dissolved Organic Matter*.
795 Academic Press, San Diego, California, pp. 509–546, 2002.

796 Bonnet, S., Moutin, T., Rodier, M., Grisoni, J. M., Louis, F., Folcher, E., Bourgeois, B., Boré,
797 J. M., and Renaud, A.: Introduction to the project VAHINE: VARIability of vertical and
798 troPHic transfer of diazotroph derived N in the south wEst Pacific, *Biogeosciences*
799 *Discuss.*, doi:10.5194/bg-2015-615, in review, 2016.

800 Bracchini, L., Tognazzi, A., Dattilo, A. M., Decembrini, F., Rossi, C., and Loisel, S. A.:
801 Sensitivity analysis of CDOM spectral slope in artificial and natural samples: an
802 application in the central eastern Mediterranean Basin, *Aquat. Sci.*, 72, 485–498, 2010.

803 Bricaud, A., Babin, M., Claustre, H., Ras, J., and Tièche, F.: Light absorption properties and
804 absorption budget of Southeast Pacific waters, *J. Geophys. Res.*, 115, C08009,
805 doi:10.1029/2009JC005517, 2010.

806 Bricaud, A., Claustre, H., Ras, J., and Oubelkheir, K.: Natural variability of phytoplanktonic
807 absorption in oceanic waters: Influence of the size structure of algal populations, *J.*
808 *Geophys. Res.*, 109, C11010, doi:10.1029/2004JC002419, 2004.

809 Bronk, D. A.: Rates of NH_4^+ uptake, intracellular transformation, and dissolved organic
810 nitrogen release in two clones of marine *Synechococcus* spp, J. Plankton Res., 21, 1337–
811 1353, 1999.

812 Carreto, J.J.: A new keto-carotenoid from the dino-flagellate *Protoperidinium depressum*
813 (Bayley) Balech, 1974, J. Plankton Res., 7, 421–423, 1985.

814 Carreto, J.I., and Carignan, M. O.: Mycosporine-like amino acids: relevant secondary
815 metabolites. Chemical and ecological aspects, Mar. Drugs, 9, 387–446, 2011.

816 Chari, N. V. H. K., Keerthi, S., Sarma, N. S., Rao Pandi, S., Chiranjeevulu, G., Kiran, R., and
817 Koduru, U.: Fluorescence and absorption characteristics of dissolved organic matter
818 excreted by phytoplankton species of western Bay of Bengal under axenic laboratory
819 condition, J. Exper. Mar. Biol. Ecol., 445, 148–155, 2013.

820 Coble, P. G.: Characterization of marine and terrestrial DOM in seawater using excitation
821 emission matrix spectroscopy, Mar. Chem., 51, 325–346, 1996.

822 Coble, P. G.: Marine optical biogeochemistry – the chemistry of ocean color, Chem. Rev.,
823 107, 402–418, 2007.

824 Davis, J., and Benner, R: Quantitative estimates of labile and semi-labile dissolved organic
825 carbon in the western Arctic Ocean: A molecular approach, Limnol. Oceanogr., 52, 2434–
826 2444, 2007.

827 Del Vecchio, R., and Blough, N. V.: Photobleaching of chromophoric dissolved organic
828 matter in natural waters: Kinetics and modelling, Mar. Chem. 78, 231–253, 2002.

829 Dupouy, C., Frouin, R., Röttgers, R., Neveux, J., Gallois, F., Panché, J. Y., Gérard, P.,
830 Fontana, C., Pinazo, C., Ouillon, S., and Minghelli-Roman, A.: Ocean color response to an
831 episode of heavy rainfall in the lagoon of New Caledonia, Proc. SPIE, 7459, Ocean
832 Remote Sensing: Methods and Applications, 74590G, doi: 10.1117/12.829251, 2009.

833 Dupouy, C., Loisel, H., Neveux, J., Brown, S. L., Moulin, C., Blanchot, J., Le Bouteiller, A.,
834 and Landry, M. R.: Microbial absorption and backscattering coefficients from in situ and
835 POLDER satellite data during an El Niño–Southern Oscillation cold phase in the equatorial
836 Pacific (180°), *J. Geophys. Res.*, 108(C12), 8138, doi:10.1029/2001JC001298, 2003.

837 Dupouy, C., Neveux, J., and André, J. M.: Spectral absorption coefficient of
838 photosynthetically active pigments in the equatorial Pacific (165°E–150°W), *Deep Sea*
839 *Res. Part II*, 44, 1881–1906, 1997.

840 Dupouy, C., Neveux, J., Dirberg, G., Röttgers, R., Tenório, M. M. B., and Ouillon, S.: Bio-
841 optical properties of the marine cyanobacteria *Trichodesmium* spp, *J. Appl. Remote Sens.*,
842 2, 1–17, 2008.

843 Dupouy, C., Petit, M., and Dandonneau, Y.: Satellite detected cyanobacteria bloom in the
844 southwestern tropical Pacific. Implication for nitrogen fixation, *Inter. J. Remote Sens.*, 8,
845 389–396, 1988.

846 Dupouy, C., Röttgers, R., Tedetti, M., Martias, C., Murakami, H., Doxaran, D., Lantoiné, F.,
847 Rodier, M., Favareto, L., Kampel, M., Goutx, M., and Frouin, R.: Influence of CDOM and
848 Particle Composition on Ocean Color of the Eastern New Caledonia Lagoon during the
849 CALIOPE Cruises, *Proc. of SPIE*, 9261, Ocean Remote Sensing and Monitoring from
850 Space, 92610M, 2014.

851 Fellman, J. B., Hood, E., and Spencer, R. G. M.: Fluorescence spectroscopy opens new
852 windows into dissolved organic matter dynamics in freshwater ecosystems: A review,
853 *Limnol. Oceanogr.*, 55, 2452–2462, 2010.

854 Foster, R. A., Subramaniam, A., and Zehr, J. P.: Distribution and activity of diazotrophs in the
855 Eastern Equatorial Atlantic, *Environ. Microbiol.*, 11, 741–750, 2009.

856 Fuchs, R., Dupouy, C., Douillet, P., Caillaud, M., Mangin, A., Pinazo, C.: Modelling the
857 impact of a La Niña event on a South West Pacific Lagoon, *Mar. Pollut. Bull.*, 64, 1596–
858 15613, 2012.

859 Grenz, C., Le Borgne, R., Fichez, R., and Torrétou, J. P.: Tropical lagoon multidisciplinary
860 investigations: An overview of the PNEC New Caledonia pilot site, *Mar. Pollut. Bull.*, 61,
861 267–268, 2010.

862 Helms, J. R., Stubbins, A., Ritchie, J. D., Minor, E. C., Kieber, D. J., and Mopper, K.:
863 Absorption spectral slopes and slope ratios as indicators of molecular weight, source and
864 photobleaching of chromophoric dissolved organic matter, *Limnol. Oceanogr.*, 53, 955–
865 969, 2008.

866 Hernes, P. J., and Benner, R.: Terrigenous organic matter sources and reactivity in the North
867 Atlantic Ocean and a comparison to the Arctic and Pacific oceans, *Mar. Chem.*, 100, 66–
868 79, 2006.

869 Ishii, S. K. L., and Boyer, T. H.: Behavior of Reoccurring PARAFAC Components in
870 Fluorescent Dissolved Organic Matter in Natural and Engineered Systems: A Critical
871 Review, *Environ. Sci. Technol.*, 46, 2006–2017, 2012.

872 Kirchman, D. L., K'nees, E., and Hodson, R.: Leucine incorporation and its potential as a
873 measure of protein synthesis by bacteria in natural waters, *Appl. Environment. Microbiol.*,
874 49, 599–607, 1985.

875 Kowalczyk, P., Durako, M. J., Young, H., Kahn, A. E., Cooper, W. J., and Gonsior, M.:
876 Characterization of dissolved organic matter fluorescence in the South Atlantic Bight with
877 use of PARAFACmodel: interannual variability, *Mar. Chem.*, 113, 182–196, 2009.

878 Kowalczyk, P., Tilstone, G. H., Zabłocka, M., Röttgers, R., and Thomas, R.: Composition of
879 dissolved organic matter along an Atlantic Meridional Transect from fluorescence
880 spectroscopy and Parallel Factor Analysis, *Mar. Chem.*, 157, 170–184, 2013.

881 Lantoiné, F., and Neveux, J.: Spatial and seasonal variations in abundance and spectral
882 characteristics of phycoerythrins in the tropical northeastern Atlantic Ocean, *Deep-Sea*
883 *Res. I*, 44, 223–246, 1997.

884 Le Bouteiller, A., Blanchot, J., and Rodier, M.: Size distribution patterns of phytoplankton in
885 the western Pacific: towards a generalization for the tropical open ocean, *Deep Sea Res.*
886 *Part A. Oceanogr. Res. Pap.*, 39, 805–823, 1992.

887 Lefort, T., Gasol, J. M.: Short-time scale coupling of picoplankton community structure and
888 single-cell heterotrophic activity in winter in coastal NW Mediterranean Sea waters. *J.*
889 *Plankton Res.*, 36, 243–258, 2014.

890 Lohrenz, S. E., Weidemann, A. D., and Tuel, M.: Phytoplankton spectral absorption as
891 influenced by community size structure and pigment composition, *J. Plankton Res.*, 25,
892 35–61, 2003.

893 Lønborg, C., Yokokawa, T., Herndl, G. J., and Álvarez-Salgado, X. A.: Production and
894 degradation of fluorescent dissolved organic matter in surface waters of the eastern north
895 Atlantic ocean, *Deep Sea Res. Part I*, 96, 28–37.

896 Lutz, V. A., Sathyendranath, S., and Head, E. J. H.: Absorption coefficient of phytoplankton:
897 Regional variations in the North Atlantic, *Mar. Ecol. Prog. Ser.*, 135, 197–213, 1996.

898 Lutz, V. A., Sathyendranath, S., Head, E., and Li, W. K. W.: Changes in the in vivo absorption
899 and fluorescence excitation spectra with growth irradiance in three species of
900 phytoplankton. *J. Plankton Res.*, 23, 555–569, 2001.

901 Marie, D., Partensky, F., Vaulot, D., and Brussaard, C. P. D.: Enumeration of phytoplankton,
902 bacteria, and viruses in marine samples. In Robinson, J. P., Darzynkiewicz, Z., Dean, P.
903 N., Orfao, A., Rabinovitch, P. S., Stewart, C. C., Tanke, H. J., Wheelless, L. L. (eds)
904 *Current Protocols in Cytometry*. John Wiley & Sons Inc., New York, pp. 11.11.1–
905 11.11.15, 1999.

906 Masotti, I., Ruiz Pino, D., and Le Bouteiller, A.: Photosynthetic characteristics of
907 *Trichodesmium* in the southwest Pacific Ocean: importance and significance, *Mar. Ecol.*
908 *Progr. Ser.*, 338, 47–59, 2007.

909 Matsuoka, A., Babin, M., Doxaran, D., Hooker, S. B., Mitchell, B. G., Bélanger, S., and
910 Bricaud, A.: A synthesis of light absorption properties of the Arctic Ocean: application to
911 semianalytical estimates of dissolved organic carbon concentrations from space,
912 *Biogeosciences*, 11, 3131–3147, 2014.

913 Morel, A.: Consequences of a *Synechococcus* bloom upon the optical properties of oceanic
914 (case 1) waters, *Limnol. Oceanogr.*, 42, 1746–1754, 1997.

915 Morel, A., Claustre, H., and Gentili, B.: The most oligotrophic subtropical zones of the global
916 ocean: similarities and differences in terms of chlorophyll and yellow substance,
917 *Biogeosciences*, 7, 3139–3151, 2010.

918 Morel, A., and Prieur, L.: Analysis of variations in ocean color, *Limnol. Oceanogr.*, 22, 709–
919 722, 1977.

920 Morel, A., Ahn, Y. H., Partensky, F., Vaultot, D., and Claustre, H.: *Prochlorococcus* and
921 *Synechococcus* - A comparative study of their optical properties in relation to their size and
922 pigmentation, *J. Mar. Res.* 51, 617–649, 1993.

923 Murphy, K. R., Stedmon, C. A., Waite, T. D., and Ruiz, G. M.: Distinguishing between
924 terrestrial and autochthonous organic matter sources in marine environments using
925 fluorescence spectroscopy, *Mar. Chem.*, 108, 40–58, 2008.

926 Nagata, T.: Production mechanisms of dissolved organic matter. In Kirchman, D. L. (ed.),
927 *Microbial Ecology of the Oceans*. Wiley-Liss, New York, pp. 121–152, 2000.

928 Nelson, N. B., and Siegel, D. A.: The Global Distribution and Dynamics of Chromophoric
929 Dissolved Organic Matter, *Annu. Rev. Mar. Sci.*, 5, 447–476, 2013.

930 Nelson, N. B., Siegel, D. A., Carlson, C. A., and Swan, C. M.: Tracing global biogeochemical
931 cycles and meridional overturning circulation using chromophoric dissolved organic
932 matter, *Geophys. Res. Lett.* 37, L03610, 2010.

933 Nelson, N. B., Siegel, D. A., and Michaels, A. F.: Seasonal dynamics of colored dissolved
934 material in the Sargasso Sea, *Deep-Sea Res. I*, 45, 931–957, 1998.

935 Neveux, J., Lantoiné, F., Vaultot, D., Marie, D., and Blanchot, J.: Phycoerythrins in the
936 southern tropical and equatorial Pacific Ocean: evidence for new cyanobacterial types, *J.*
937 *Geophys. Res.* 104, 3311–3321, 1999.

938 Neveux, J., Tenório, M. M. B., Jacquet, S., Torrétón, J.-P., Douillet, P., Ouillon, S., Dupouy,
939 C.: Chlorophylls and Phycoerythrins as Markers of Environmental Forcings Including
940 Cyclone Erica Effect (March 2003) on Phytoplankton in the Southwest Lagoon of New
941 Caledonia and Oceanic Adjacent Area, *Intern. J. Oceanogr.*, doi:10.1155/2009/232513,
942 2009.

943 Nieto-Cid, M., Álvarez-Salgado, X. A., and Pérez, F. F.: Microbial and photochemical
944 reactivity of fluorescent dissolved organic matter in a coastal upwelling system, *Limnol.*
945 *Oceanogr.*, 51, 1391–1400, 2006.

946 Organelli, E., Bricaud, A., Antoine, D., and Matsuoka, A.: Seasonal dynamics of light
947 absorption by chromophoric dissolved organic matter (CDOM) in the NW Mediterranean
948 Sea (BOUSSOLE site), *Deep-Sea Res. I*, 91, 72–85, 2014.

949 Ortega-Retuerta, E., Frazer, T. K., Duarte, C. M., Ruiz-Halpern, S., Tovar-Sanchez, A.,
950 Arrieta, J. M., and Reche, I.: Biogeneration of chromophoric dissolved organic matter by
951 bacteria and krill in the Southern Ocean, *Limnol. Oceanogr.*, 54, 1941–1950, 2009.

952 Ouillon, S., Douillet, P., Lefebvre, J. P., Le Gendre, R., Jouon, A., Bonneton, P., Fernandez, J.
953 M., Chevillon, C., Magand, O., Lefèvre, J., Le Hir, P., Laganier, R., Dumas, F.,
954 Marchesiello, P., Bel Madani, A., Andréfouët, S., Panché, J. Y., and Fichez, R.: Circulation

955 and suspended sediment transport in a coral reef lagoon: The south-west lagoon of New
956 Caledonia, *Mar. Pollut. Bull.*, 61, 269–296, 2010.

957 Para, J., Coble, P. G., Charrière, B., Tedetti, M., Fontana, C., and Sempéré, R.: Fluorescence
958 and absorption properties of chromophoric dissolved organic matter (CDOM) in coastal
959 surface waters of the northwestern Mediterranean Sea, influence of the Rhône River,
960 *Biogeosciences*, 7, 4083–40103, 2010.

961 Pavlov, A. K., Silyakova, A., Granskog, M. A., Bellerby, R. G. J., Engel, A., Schulz, K. G.,
962 and Brussaard C. P. D.: Marine CDOM accumulation during a coastal Arctic mesocosm
963 experiment: No response to elevated pCO₂ levels, *J. Geophys. Res. Biogeosci.*, 119, 1216–
964 1230, doi:10.1002/2013JG002587, 2014.

965 Pujo-Pay, M., and Raimbault, P.: Improvement of the Wet-Oxidation Procedure for
966 Simultaneous Determination of Particulate Organic Nitrogen and Phosphorus Collected on
967 Filters, *Mar. Ecol. Prog. Ser.*, 105, 203–207, 1994.

968 Rochelle-Newall, E., Delille, B., Frankignoulle, M., Gattuso, J. P., Jacquet, S., Riebesell, U.,
969 Terbrüggen A., and Zondervan, I.: Chromophoric dissolved organic matter in experimental
970 mesocosms maintained under different pCO₂ levels, *Mar. Ecol. Prog. Ser.*, 272, 25–31,
971 2004.

972 Rochelle-Newall, E. J., and Fisher, T. R.: Production of chromophoric dissolved organic
973 matter fluorescence in marine and estuarine environments: an investigation into the role of
974 phytoplankton, *Mar. Chem.*, 77, 7–21, 2002.

975 Rochelle-Newall, E. J., Fisher, T. R., Fan, C., and Glibert, P. M.: Dynamics of chromophoric
976 dissolved organic matter and dissolved organic carbon in experimental mesocosms, *Int. J.*
977 *Remote Sens.* 20, 627– 641, 1999.

978 Rodier, M., and Le Borgne, R.: Population and trophic dynamics of *Trichodesmium thiebautii*
979 in the SE lagoon of New Caledonia. Comparison with *T. erythraeum* in the SW lagoon,
980 Mar. Pollut. Bull., 61, 349–359, 2010.

981 Romera-Castillo, C., Sarmiento, H., Álvarez-Salgado, X. A., Gasol, J. M., and Marrasé, C.:
982 Production of chromophoric dissolved organic matter by marine phytoplankton, Limnol.
983 Oceanogr., 55, 446–454, 2010.

984 Romera-Castillo, C., Sarmiento, H., Álvarez-Salgado, X. A., Gasol, J. M., and Marrasé, C.:
985 Net Production and Consumption of Fluorescent Colored Dissolved Organic Matter by
986 Natural Bacterial Assemblages Growing on Marine Phytoplankton Exudates, Appl.
987 Environment. Microbiol., 77, 7490–7498, 2011.

988 Röttgers, R., and Doerffer, R.: Measurements of optical absorption by chromophoric
989 dissolved organic matter using a point-source integrating-cavity absorption meter, Limnol.
990 Oceanogr. Met., 126–135, 2007.

991 Röttgers, R., Dupouy, C., Taylor, B. B., Bracher, A., and Wozniak, S. B.: Mass-specific light
992 absorption coefficients of natural aquatic particles in the near-infrared spectral region,
993 Limnol. Oceanogr., 59, 1449–1460, 2014.

994 Röttgers, R., Häse, C., and Doerffer, R.: Determination of the particulate absorption of
995 microalgae using a point-source integrating-cavity absorption meter: verification with a
996 photometric technique, improvements for pigment bleaching and correction for chlorophyll
997 fluorescence, Limnol. Oceanogr. Methods, 5, 1–12, 2007.

998 Röttgers, R., and Koch, B. P.: Spectroscopic detection of a ubiquitous dissolved pigment
999 degradation product in subsurface waters of the global ocean, Biogeosciences, 9, 2585–
1000 2596, 2012.

1001 Sempéré, R., Para, J., Tedetti, M., Charrière, B., and Mallet, M.: Variability of solar radiation
1002 and CDOM in surface coastal waters of the Northwestern Mediterranean Sea. *Photochem.*
1003 *Photobiol.*, 91, 851–861, 2015.

1004 Siegel, D. A., Maritorena, S., Nelson, N. B., and Behrenfeld, M. J.: Independence and
1005 interdependencies of global ocean color properties; Reassessing the bio-optical
1006 assumption, *J. Geophys. Res.*, 110, C07011, doi:10.1029/2004JC002527, 2005.

1007 Siegel, D. A., Maritorena, S., Nelson, N. B., Hansell, D. A., and Lorenzi-Kayser, M.: Global
1008 distribution and dynamics of colored dissolved and detrital organic materials, *J. Geophys.*
1009 *Res.*, 107(C12), 3228, doi:10.1029/2001JC000965, 2002.

1010 Smith, D. C, and Azam, F.: A simple, economical method for measuring bacterial protein
1011 synthesis rates in sea water using 3H-Leucine, *Mar. Microb. Food Webs*, 6, 107–114,
1012 1992.

1013 Sohrin, R., and Sempéré R.: Temporal variation in total organic carbon in the Northeast
1014 Atlantic in 2000–2001, *J. Geophys. Res.* 110, C10S90, doi: 10.1029/2004JC002731, 2005.

1015 Stedmon, C. A., and Bro, R.: Characterizing dissolved organic matter fluorescence with
1016 parallel factor analysis: a tutorial, *Limnol. Oceanogr. Met.*, 6, 572–579, 2008.

1017 Stedmon, C. A., and Cory, R. M.: Biological Origins and Fate of Fluorescent Dissolved
1018 Organic Matter in Aquatic Environments. In *Aquatic Organic Matter Fluorescence*. Eds
1019 PG Coble, J Lead, A. Baker, DM Reynolds, RGM Spencer. Cambridge University Press,
1020 New York, pp. 278–299, 2014.

1021 Stedmon, C. A., Markager, S., and Bro, R.: Tracing dissolved organic matter in aquatic
1022 environments using a new approach to fluorescence spectroscopy, *Mar. Chem.*, 82, 239–
1023 254, 2003.

1024 Steinberg, D. K., Nelson, N., Carlson, C. A., and Prusak, A. C.: Production of chromophoric
1025 dissolved organic matter (CDOM) in the open ocean by zooplankton and the colonial
1026 cyanobacterium *Trichodesmium* spp, Mar. Ecol. Prog. Ser., 267, 45–56, 2004.

1027 Stramski, D., and Mobley, C. D.: Effects of microbial particles on oceanic optics: A database
1028 of single-particle optical properties. Limnol. Oceanogr., 42, 538–549, 1997.

1029 Stuart, V., Sathyendranath, S., Platt, T., Maass, H., and Irwin, B. D.: Pigment and species
1030 composition of natural phytoplankton populations: Effect on the absorption spectra, J.
1031 Plankton Res., 20, 187–217, 1998.

1032 Subramaniam, A., Carpenter, E. J., Karentz, D., and Falkowski, P. G.: Bio-optical properties
1033 of the marine diazotrophic cyanobacteria *Trichodesmium* spp. I. Absorption and
1034 photosynthetic action spectra, Limnol. Oceanogr., 44, 608–617, 1999.

1035 Swan, C., M., Siegel, D. A., Nelson, N. B., Carlson, C. A., and Nasir, E.: Biogeochemical and
1036 hydrographic controls on chromophoric dissolved organic matter distribution in the Pacific
1037 Ocean, Deep-Sea Res. I Oceanogr. Res. Pap., 56, 2175–2192, 2009.

1038 Swan, C. M., Siegel, D. A., Nelson, N. B., and Kostadinov, T. S.: The effect of surface
1039 irradiance on the absorption spectrum of chromophoric dissolved organic matter in the
1040 global ocean, Deep-Sea Res. I, 63, 52–64, 2012.

1041 Tedetti, M., Charrière, B., Bricaud, A., Para, J., Raimbault, P., and Sempéré, R.: Distribution
1042 of normalized waterleaving radiances at UV and visible wave bands in relation with
1043 chlorophyll a and colored detrital matter content in the southeast Pacific, J. Geophys. Res.,
1044 115, C02010, doi:10.1029/2009JC005289, 2010.

1045 Tedetti, M., Longhitano, R., Garcia, N., Guigue, C., Ferretto, N., and Goutx, M.: Fluorescence
1046 properties of dissolved organic matter in coastal Mediterranean waters influenced by a
1047 municipal sewage effluent (Bay of Marseilles, France), Environ. Chem., 9, 438–449, 2012.

1048 Tedetti, M., Sempéré, R., Vasilkov, A., Charrière, B., Nérini, D., Miller, W., Kawamura, K.,
1049 and Raimbault, P.: High penetration of ultraviolet radiation in the south east Pacific waters,
1050 *Geophys. Res. Lett.*, 34, L12610, doi:10.1029/2007 GL029823, 2007.

1051 Tilstone, G. H., Peters, S. W. M., van derWoerd, H. J., Eleveld, M. A., Ruddick, K.,
1052 Schönfeld, W., Krasemann, H., Martinez-Vicente, V., Blondeau-Patissier, D., Röttgers, R.,
1053 Sørensen, K., Jørgenseng, P. V., and Shutler, J. D.: Variability in specific-absorption
1054 properties and their use in a semianalytical ocean colour algorithm for MERIS in north sea
1055 andwestern English channel coastal waters, *Remote Sen. Environ.*, 118, 320–338, 2012.

1056 Turk-Kubo, K. A., Frank, I. E., Hogan, M. E., Desnues, A., Bonnet, S., and Zehr, J. P.:
1057 Diazotroph community succession during the VAHINE mesocosms experiment (New
1058 Caledonia Lagoon), *Biogeosciences*, 12, 7435–7452, 2015.

1059 Twardowski, M. S., Boss, E., Sullivan, J. M., and Donaghay, P. L.: Modeling the spectral
1060 shape of absorption by chromophoric dissolved organic matter, *Mar. Chem.*, 89, 69–88,
1061 2004.

1062 Vernet, M., and Whitehead, K.: Release of ultraviolet-absorbing compounds by the red-tide
1063 dinoflagellate *Lingulodinium polyedra*, *Mar. Biol.*, 127, 35–44, 1996.

1064 Whitehead, K., and Vernet, M.: Influence of mycosporine-like amino acids (MAAs) on UV
1065 absorption by particulate and dissolved organic matter in La Jolla Bay, *Limnol. Oceanogr.*,
1066 45,1788–1796, 2000.

1067 Wyman, M.: An in vivo method for the estimation of phycoerythrin concentrations in marine
1068 cyanobacteria (*Synechococcus* spp.), *Limnol. Oceanogr.*, 37, 1300–1306, 1992.

1069 Wozniak, B., Dera, J., Ficek, D., Machrowski, R., Kaczmarek, S., Ostrowska, M., and
1070 Koblentz-Mischke, O. I.: Modelling the influence of acclimation on the absorption
1071 properties of marine phytoplankton, *Oceanologia*, 41, 187–210, 1999.

1072 Xing, X., Claustre, H., Wang, H., Poteau, A., and D'Ortenzio, F.: Seasonal dynamics in
1073 colored dissolved organic matter in the Mediterranean Sea: patterns and drivers, *Deep-Sea*
1074 *Res. I*, 83, 93–101, 2014.

1075 Yamashita, Y., Jaffe, R., Maie, N., and Tanoue, E.: Assessing the dynamics of dissolved
1076 organic matter (DOM) in coastal environments by excitation emission matrix fluorescence
1077 and parallel factor analysis (EEM-PARAFAC), *Limnol. Oceanogr.*, 53, 1900–1908, 2008.

1078 Yamashita, Y., Nosaka, Y., Suzuki, K., Ogawa, H., Takahashi, K., and Saito H:
1079 Photobleaching as a factor controlling spectral characteristics of chromophoric dissolved
1080 organic matter in open ocean, *Biogeosciences*, 10, 7207–7217, 2013.

1081 Yamashita, Y., Tanoue, E.: In situ production of chromophoric dissolved organic matter in
1082 coastal environments, *Geophys. Res. Lett.*, 31(14), 1–4. doi:10.1029/2004GL019734,
1083 2004.

1084

1085

1086

1087

1088

1089

1090

1091

1092

1093

1094

1095

1096

1097

1098 **Figure captions**

1099

1100 **Figure 1.** Location of the site of the VAHINE mesocosm experiment at the exit of the New
1101 Caledonian coral lagoon, 28 km off the coast of New Caledonia, in the South West Pacific
1102 (Ocean Data View software version 4.6.5, Schlitzer, R., <http://odv.awi.de>, 2014, and Google
1103 Earth).

1104

1105 **Figure 2.** Pictures of the VAHINE mesocosms deployed at the exit of the New Caledonian
1106 coral lagoon.

1107

1108 **Figure 3.** Evolution of a) total chlorophyll *a* (TChl *a*) and b) phycoerythrin concentrations
1109 ($\mu\text{g L}^{-1}$), c) total organic carbon (TOC), d) particulate organic nitrogen (PON) and e)
1110 dissolved organic nitrogen (DON) concentrations (μM) and f) bacterial production (BP) (ng C
1111 $\text{L}^{-1} \text{h}^{-1}$) in the mesocosm M1 and in the surrounding waters (OUT) at 1, 6 and 12 m depths
1112 (except phycoerythrin and TOC concentrations, determined only at 6 m depth) over the course
1113 of the 23-day experiment. Dots are mean values with standard deviation from duplicate
1114 measurements, except for phycoerythrin. For TChl *a*, standard deviations are comprised
1115 within dots. Black line represents the depth-averaged values. P1: first part of the experiment,
1116 from day 5 to day 14; P2: second part of the experiment, from day 15 to day 23.

1117

1118 **Figure 4.** Evolution of the abundance of a) diatoms-diazotrophs associations (DDAs) and b)
1119 unicellular diazotrophic cyanobacteria Group C (UCYN-C) ($\times 10^3 \text{ nifH copies L}^{-1}$) in the
1120 mesocosm M1 and in the surrounding waters (OUT), and c) total diatoms ($\times 10^3 \text{ cell L}^{-1}$), d)
1121 *Synechococcus* spp., e) *Prochlorococcus* spp., f) picoeukaryotes and g) nanoeukaryotes ($\times 10^3$
1122 cell mL^{-1}) in the mesocosm M1 only, over the course of the 23-day experiment.

1123 *Synechococcus* spp., *Prochlorococcus* spp., picoeukaryotes and nanoeukaryotes were
1124 determined at 1, 6 and 12 m depths, while DDAs, UCYN-C and total diatoms were
1125 determined solely at 6 m depth. For DDAs and UCYN-C, dots are mean values with standard
1126 deviation from duplicate measurements. Black line represents the depth-averaged values. P1:
1127 first part of the experiment, from day 5 to day 14; P2: second part of the experiment, from day
1128 15 to day 23. Detailed data about diazotrophs (DDAs and UCYN-C) are found in Turk-Kubo
1129 et al. (2015).

1130

1131 **Figure 5.** Absorption spectra of chromophoric dissolved organic matter (CDOM) and
1132 particulate matter over the ranges 370-720 nm of samples collected in the mesocosm M1 at 1,
1133 6 and 12 m depths and in the surrounding waters at 1 m depth. Black lines represent the
1134 average of all spectra and shaded areas represent the measured minimal and maximal values.
1135 Peaks and shoulders are reported for particulate matter.

1136

1137 **Figure 6.** Evolution of a) absorption coefficient of CDOM at 370 nm [$a_g(370)$ in m^{-1}], b)
1138 absorption coefficient of CDOM at 442 nm [$a_g(442)$ in m^{-1}], c) spectral slope of CDOM
1139 absorption in the range 370-500 nm (S_g in nm^{-1}), d) absorption coefficient of particulate
1140 matter at 442 nm [$a_p(442)$ in m^{-1}] and e) absorption coefficient of particulate matter at 676 nm
1141 [$a_p(676)$ in m^{-1}] in the mesocosm M1 at 1, 6 and 12 m depths and in the surrounding waters
1142 (OUT) at 1 m depth over the course of the 23-day experiment. Dots are mean values with
1143 standard deviation from duplicate measurements, except for S_g . Black line represents the
1144 depth-averaged values. P1: first part of the experiment, from day 5 to day 14; P2: second part
1145 of the experiment, from day 15 to day 23.

1146

1147 **Figure 7.** Spectral characteristics of the three FDOM components (C1-C3) validated by the
1148 PARAFAC model for 130 EEMs of samples collected in the mesocosm M1 at 1, 6 and 12 m
1149 depths and in the surrounding waters at 1 m depth over the course of the 23-day experiment.
1150 Both contour (left column) and line (right column) plots are depicted. The line plots show the
1151 excitation (left side) and emission (right side) fluorescence spectra. The dotted grey lines
1152 correspond to split half validation results. The excitation and emission maxima (λ_{Ex} and λ_{Em})
1153 of each component are given.

1154
1155 **Figure 8.** Evolution of the fluorescence intensities (QSU) of the three FDOM components: a)
1156 humic-like, b) tryptophan-like and c) tyrosine-like fluorophores in the mesocosm M1 at 1, 6
1157 and 12 m depths over the course of the 23-day experiment (actually up to day 20 and not to
1158 day 23). Dots are mean values with standard deviation from duplicate measurements. Black
1159 line represents the depth-averaged values. P1: first part of the experiment, from day 5 to day
1160 14; P2: second part of the experiment, from day 15 to day 23. Fluorescence intensities in the
1161 surrounding waters (OUT) at 1 m depth were determined on only few samples at the
1162 beginning and the end of the experiment and are thus not presented here.

1163
1164 **Figure 9.** Linear relationships between absorption coefficient of CDOM at 370 nm [$a_g(370)$
1165 in m^{-1}] or absorption coefficient of particulate matter at 442 nm [$a_p(442)$ in m^{-1}] and
1166 *Synechococcus* spp. abundance ($\times 10^3$ cell mL^{-1}) for samples collected in the mesocosm M1
1167 from day 5 to day 20, i.e. from the day after the dissolved inorganic phosphorus fertilization
1168 to almost the end of the experiment (P1 + P2) ($n = 36$).

1169 **Table 1.** Mean values and associated standard deviations of chromophoric, biogeochemical and biological parameters of samples
 1170 collected in the mesocosm M1 and in the surrounding waters (OUT) during the first part of the experiment, i.e. from day 5 to day
 1171 14 (P1), and during the second part of the experiment, i.e. from day 15 to day 23 (P2). The means which have different letters (*a*,
 1172 *b*, *c* or *d*) are significantly different (ANOVA, $p < 0.05$). M1-P2 values in bold are significantly different from M1-P1, OUT-P1
 1173 and OUT-P2 values.

	M1-P1 (<i>n</i>)	M1-P2 (<i>n</i>)	OUT-P1 (<i>n</i>)	OUT-P2 (<i>n</i>)
TChl <i>a</i> ($\mu\text{g L}^{-1}$)	0.19 \pm 0.05 ^{<i>a</i>} (28)	0.42 \pm 0.14^{<i>b</i>} (27)	0.21 \pm 0.03 ^{<i>a</i>} (25)	0.30 \pm 0.07 ^{<i>c</i>} (25)
Phycoerythrin ($\mu\text{g L}^{-1}$)	0.17 \pm 0.09 ^{<i>a</i>} (9)	0.24 \pm 0.09 ^{<i>a</i>} (9)	0.19 \pm 0.08 ^{<i>a</i>} (10)	0.42 \pm 0.19 ^{<i>b</i>} (9)
TOC (μM)	66.5 \pm 2.1 ^{<i>a</i>} (9)	69.7 \pm 4.3 ^{<i>b</i>} (9)	66.6 \pm 2.8 ^{<i>a</i>} (9)	67.7 \pm 1.5 ^{<i>a,b</i>} (7)
PON (μM)	0.81 \pm 0.13 ^{<i>a</i>} (30)	1.10 \pm 0.21^{<i>b</i>} (27)	0.71 \pm 0.06 ^{<i>c</i>} (30)	0.87 \pm 0.13 ^{<i>a</i>} (27)
DON (μM)	5.5 \pm 1.4 ^{<i>a</i>} (29)	4.8 \pm 0.6 ^{<i>a</i>} (22)	5.0 \pm 0.4 ^{<i>a</i>} (29)	5.3 \pm 1.8 ^{<i>a</i>} (23)
BP ($\text{ng C L}^{-1} \text{ h}^{-1}$)	157 \pm 49 ^{<i>a</i>} (30)	348 \pm 142^{<i>b</i>} (27)	135 \pm 24 ^{<i>a</i>} (30)	256 \pm 60 ^{<i>c</i>} (27)
DDAs ($\times 10^3$ <i>nifH</i> copies L ⁻¹)	120 \pm 45 ^{<i>a,b</i>} (5)	54 \pm 31 ^{<i>a</i>} (6)	227 \pm 189 ^{<i>b,c</i>} (5)	200 \pm 220 ^{<i>a,c</i>} (3)
UCYN-C ($\times 10^3$ <i>nifH</i> copies L ⁻¹)	4.5 \pm 7.6 ^{<i>a</i>} (4)	64 \pm 24^{<i>b</i>} (6)	1.2 \pm 0.8 ^{<i>a</i>} (5)	2.9 \pm 1.7 ^{<i>a</i>} (3)
Total diatoms ($\times 10^3$ cell L ⁻¹)	17 \pm 9 ^{<i>a</i>} (5)	44 \pm 37 ^{<i>a</i>} (5)	<i>nd</i>	<i>nd</i>
<i>Synechococcus</i> ($\times 10^3$ cell mL ⁻¹)	41 \pm 20 ^{<i>a</i>} (24)	88 \pm 14^{<i>b</i>} (23)	<i>nd</i>	<i>nd</i>
<i>Prochlorococcus</i> ($\times 10^3$ cell mL ⁻¹)	12 \pm 6 ^{<i>a</i>} (24)	15 \pm 3 ^{<i>a</i>} (23)	<i>nd</i>	<i>nd</i>
Picoeukaryotes ($\times 10^3$ cell mL ⁻¹)	1.5 \pm 0.8 ^{<i>a</i>} (24)	2.4 \pm 0.6^{<i>b</i>} (23)	<i>nd</i>	<i>nd</i>
Nano-eukaryotes ($\times 10^3$ cell mL ⁻¹)	0.9 \pm 0.4 ^{<i>a</i>} (24)	1.5 \pm 0.4^{<i>b</i>} (23)	<i>nd</i>	<i>nd</i>
$a_g(370)$ (m^{-1})	0.046 \pm 0.004 ^{<i>a</i>} (30)	0.058 \pm 0.009^{<i>b</i>} (27)	0.049 \pm 0.005 ^{<i>a,c</i>} (9)	0.052 \pm 0.006 ^{<i>c</i>} (9)
$a_g(442)$ (m^{-1})	0.013 \pm 0.001 ^{<i>a</i>} (30)	0.016 \pm 0.003 ^{<i>b</i>} (27)	0.015 \pm 0.002 ^{<i>a,c</i>} (9)	0.015 \pm 0.001 ^{<i>c,b</i>} (9)
S_g (nm^{-1})	0.0172 \pm 0.001 ^{<i>a,b</i>} (30)	0.0174 \pm 0.001 ^{<i>b</i>} (27)	0.0169 \pm 0.001 ^{<i>a</i>} (9)	0.0169 \pm 0.001 ^{<i>a</i>} (9)
$a_p(442)$ (m^{-1})	0.014 \pm 0.004 ^{<i>a</i>} (30)	0.022 \pm 0.004^{<i>b</i>} (27)	0.015 \pm 0.002 ^{<i>a</i>} (9)	0.018 \pm 0.002 ^{<i>c</i>} (9)
$a_p(676)$ (m^{-1})	0.005 \pm 0.002 ^{<i>a</i>} (30)	0.009 \pm 0.002 ^{<i>b</i>} (27)	0.005 \pm 0.001 ^{<i>a</i>} (9)	0.008 \pm 0.001 ^{<i>b</i>} (9)
Humic-like (QSU)	4.47 \pm 0.76 ^{<i>a</i>} (30)	4.45 \pm 1.09 ^{<i>a</i>} (18)	<i>nd</i>	<i>nd</i>
Tryptophan-like (QSU)	7.68 \pm 1.17 ^{<i>a</i>} (30)	8.07 \pm 2.07 ^{<i>a</i>} (18)	<i>nd</i>	<i>nd</i>
Tyrosine-like (QSU)	6.57 \pm 1.21 ^{<i>a</i>} (28)	5.49 \pm 0.83^{<i>b</i>} (18)	<i>nd</i>	<i>nd</i>

1174 *nd*: not determined; TChl *a*: total chlorophyll *a* concentration; TOC: total organic carbon concentration; PON and DON: particulate and dissolved organic
 1175 nitrogen concentrations; BP: bacterial production; DDAs: diatoms-diazotrophs associations; UCYN-C: unicellular diazotrophic cyanobacteria Group C;
 1176 $a_g(370)$ and $a_g(442)$: absorption coefficients of CDOM at 370 and 442 nm; S_g : spectral slope of CDOM; $a_p(442)$ and $a_p(676)$: absorption coefficients of

1177 particulate matter at 442 and 676 nm; Humic-like, tryptophan-like and tyrosine-like: fluorescence intensity of humic-like, tryptophan-like and tyrosine-like
1178 FDOM fluorophores. Detailed data about diazotrophs (DDAs and UCYN-C) are found in Turk-Kubo et al. (2015).
1179
1180
1181
1182
1183
1184
1185
1186

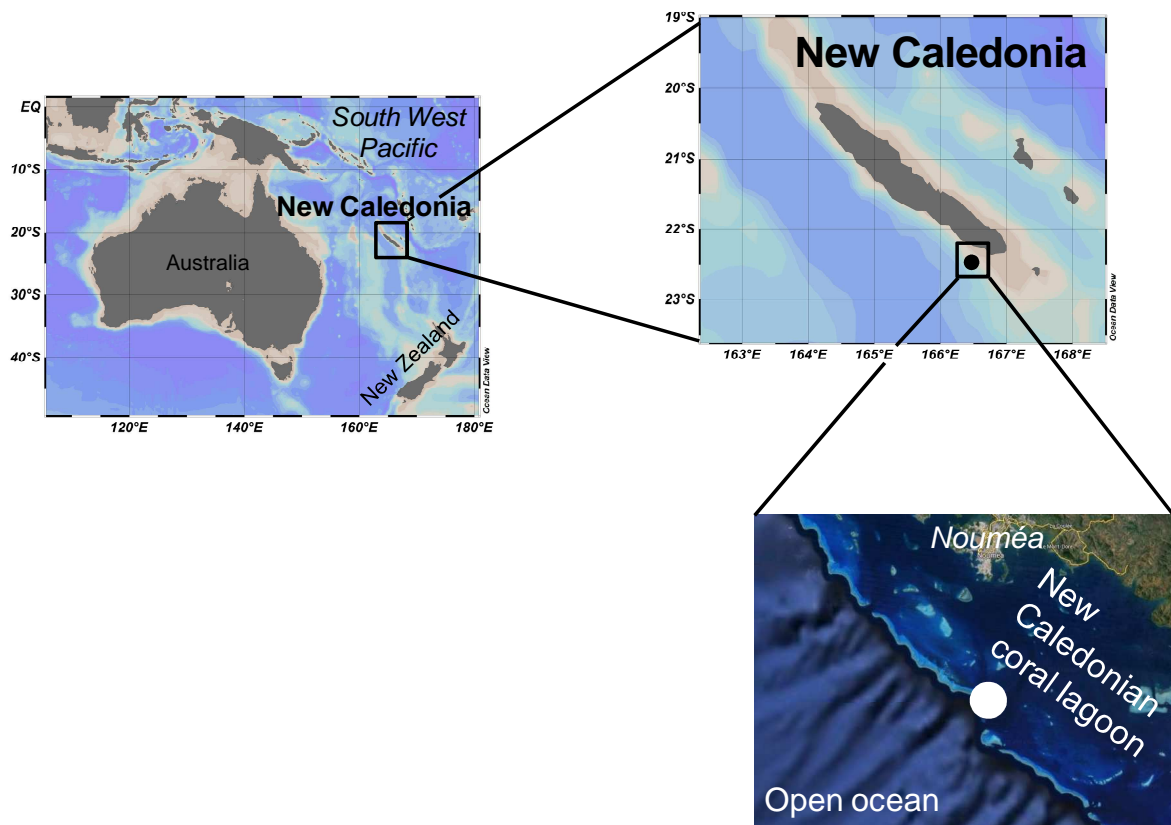
1187 **Table 2.** Pearson's correlation coefficients (r) of linear regressions between the chromophoric and the biogeochemical/biological
 1188 parameters of samples collected in the mesocosm M1 from day 5 to day 20, i.e. from the day after the dissolved inorganic phosphorus
 1189 fertilization to almost the end of the experiment (P1 + P2) ($n = 36$).

	$a_g(370)$	$a_g(442)$	S_g	$a_p(442)$	$a_p(676)$	Humic	Trypto.	Tyrosine
$a_g(442)$	0.90							
S_g	0.22	-0.15						
$a_p(442)$	0.61	0.52	0.23					
$a_p(676)$	0.62	0.53	0.30	0.93				
Humic	0.42	0.36	0.13	0.22	0.10			
Trypto.	0.28	0.24	0.28	0.17	0.16	0.67		
Tyrosine	-0.09	-0.25	0.11	-0.28	-0.39	0.48	0.20	
TChl a	0.68	0.60	0.32	0.86	0.88	0.22	0.21	-0.33
Phyco.*	0.45	0.42	0.11	0.74	0.73	0.05	0.00	-0.35
TOC*	0.35	0.16	0.63	0.57	0.59	0.52	0.43	0.28
PON	0.71	0.58	0.29	0.75	0.70	0.43	0.29	0.04
DON	-0.30	-0.23	-0.13	-0.14	-0.04	-0.26	-0.10	-0.14
BP	0.75	0.72	0.10	0.78	0.72	0.43	0.32	-0.12
DDAs*	-0.44	-0.38	-0.52	-0.85	-0.78	0.20	0.05	0.60
UCYN-C*	0.73	0.67	0.55	0.90	0.85	0.15	0.23	-0.47
Diatoms*	-0.07	-0.08	0.40	0.49	0.47	-0.85	-0.74	-0.88
<i>Synecho.</i>	0.76	0.76	0.08	0.83	0.76	0.35	0.29	-0.27
<i>Prochlo.</i>	0.42	0.47	0.08	0.57	0.50	0.13	0.03	0.00
Picoeuka.	0.52	0.62	-0.07	0.71	0.58	0.40	0.34	-0.25
Nanoeuka.	0.48	0.45	0.01	0.65	0.58	0.11	0.01	-0.35

1190 Correlation coefficients (r) in bold are very highly significant ($p < 0.0001$). * Correlations determined on a lower number of samples (n): 15 for Phyco. and TOC, 10 for
 1191 DDAs, 9 for UCYN-C and 8 for diatoms. $a_g(370)$ and $a_g(442)$: absorption coefficients of CDOM at 370 and 442 nm (m^{-1}); S_g : spectral slope of CDOM; $a_p(442)$ and
 1192 $a_p(676)$: absorption coefficients of particulate matter at 442 and 676 nm (m^{-1}); Humic: fluorescence intensity of humic-like fluorophore (QSU); Trypto.: fluorescence
 1193 intensity of tryptophan-like fluorophore (QSU); Tyrosine: fluorescence intensity of tyrosine-like fluorophore (QSU); TChl a : total chlorophyll a concentration ($\mu g L^{-1}$);
 1194 Phyco.: phycoerythrin concentration ($\mu g L^{-1}$); TOC: total organic carbon concentration (μM); PON and DON: particulate and dissolved organic nitrogen concentrations
 1195 (μM); BP: bacterial production ($ng C L^{-1} h^{-1}$); DDAs: diatoms-diazotrophs associations ($nifH$ copies L^{-1}); UCYN-C: unicellular diazotrophic cyanobacteria Group C ($nifH$)

1196 copies L⁻¹); Diatoms: total diatoms (cell L⁻¹); *Synecho.*: *Synechococcus* spp. (cell mL⁻¹); *Prochlo.*: *Prochlorococcus* spp. (cell mL⁻¹); Picoeuka.: Picoeukaryote (cell mL⁻¹);
1197 Nanoeuka.: Nanoeukaryote (cell mL⁻¹). Detailed data about diazotrophs (DDAs and UCYN-C) are found in Turk-Kubo et al. (2015).
1198
1199
1200
1201
1202
1203
1204
1205
1206
1207
1208
1209
1210
1211
1212
1213
1214
1215
1216
1217
1218
1219
1220
1221
1222
1223
1224
1225
1226
1227
1228

1229
1230
1231
1232
1233



1234
1235
1236
1237
1238
1239
1240
1241
1242
1243
1244
1245
1246
1247

Figure 1

1248
1249
1250
1251
1252
1253
1254
1255
1256
1257
1258
1259
1260
1261
1262
1263
1264
1265
1266
1267
1268
1269
1270
1271
1272
1273
1274
1275
1276
1277
1278
1279
1280
1281



Figure 2

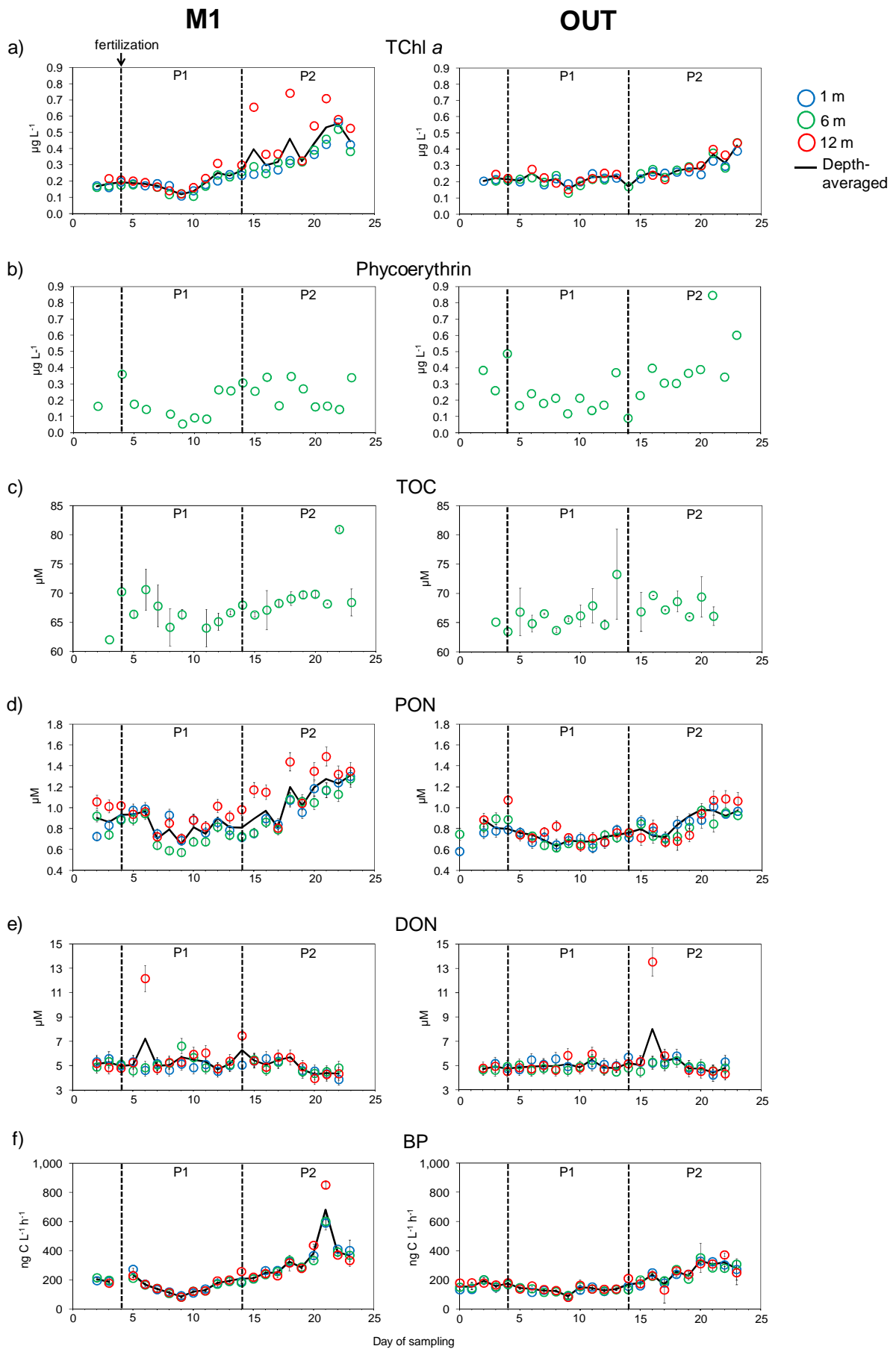
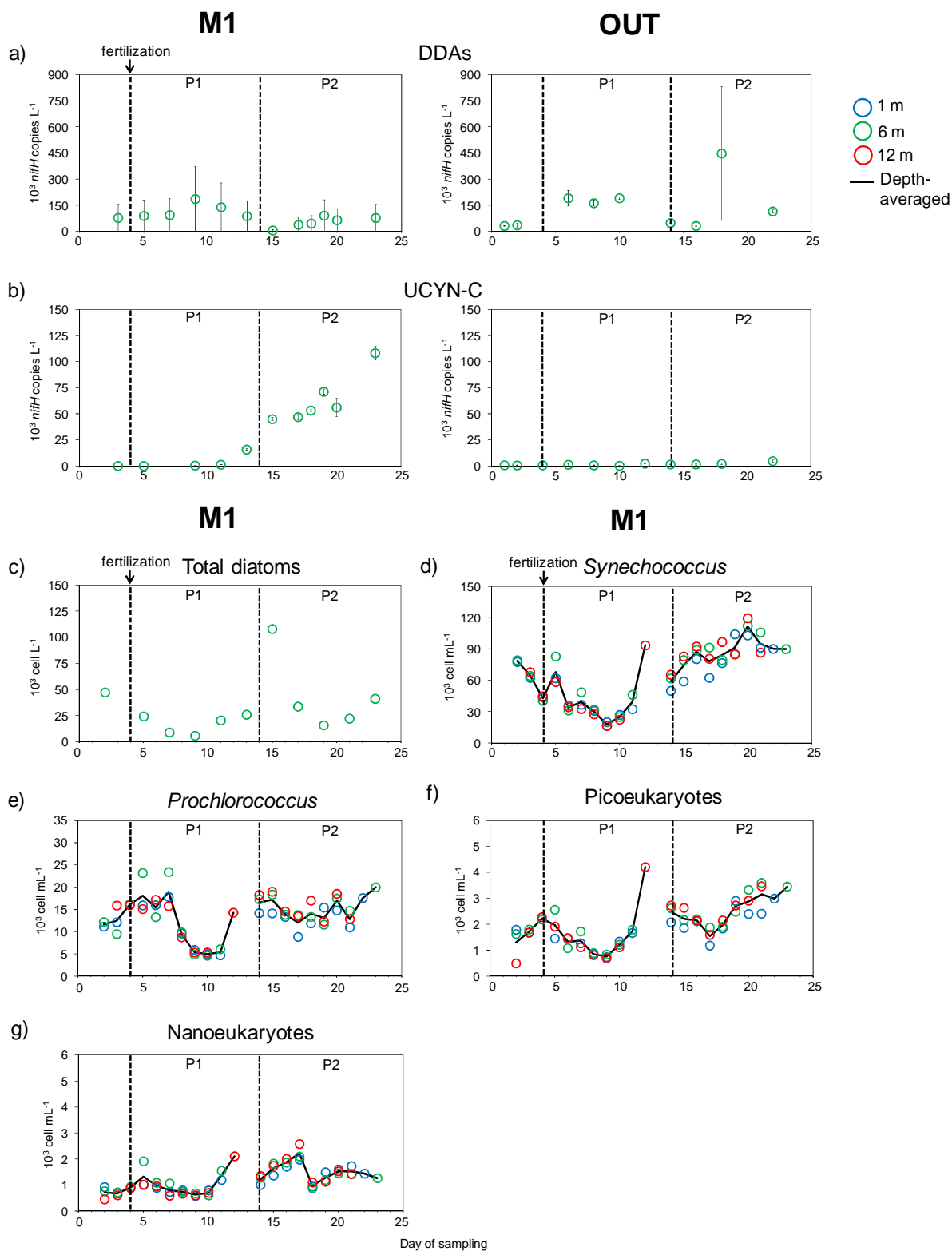


Figure 3



1284

1285

1286

1287

Figure 4

1288
1289
1290
1291
1292
1293
1294
1295
1296
1297
1298
1299
1300
1301
1302
1303
1304
1305
1306
1307
1308
1309
1310
1311
1312
1313
1314
1315
1316
1317
1318
1319
1320
1321

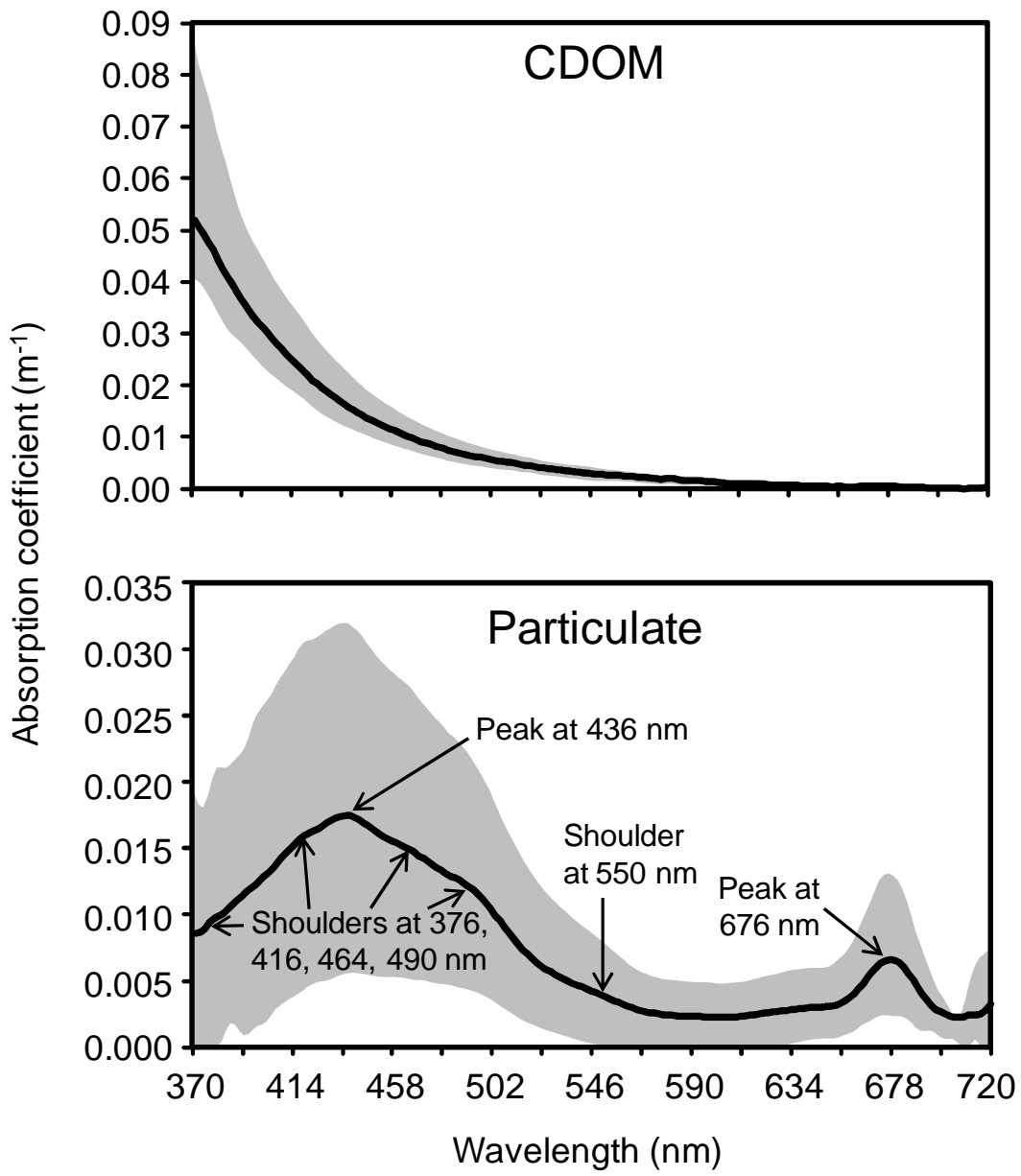


Figure 5

1322
 1323
 1324
 1325
 1326
 1327
 1328
 1329
 1330
 1331
 1332
 1333
 1334
 1335
 1336
 1337
 1338
 1339
 1340
 1341
 1342
 1343
 1344
 1345
 1346
 1347
 1348
 1349
 1350
 1351
 1352
 1353
 1354

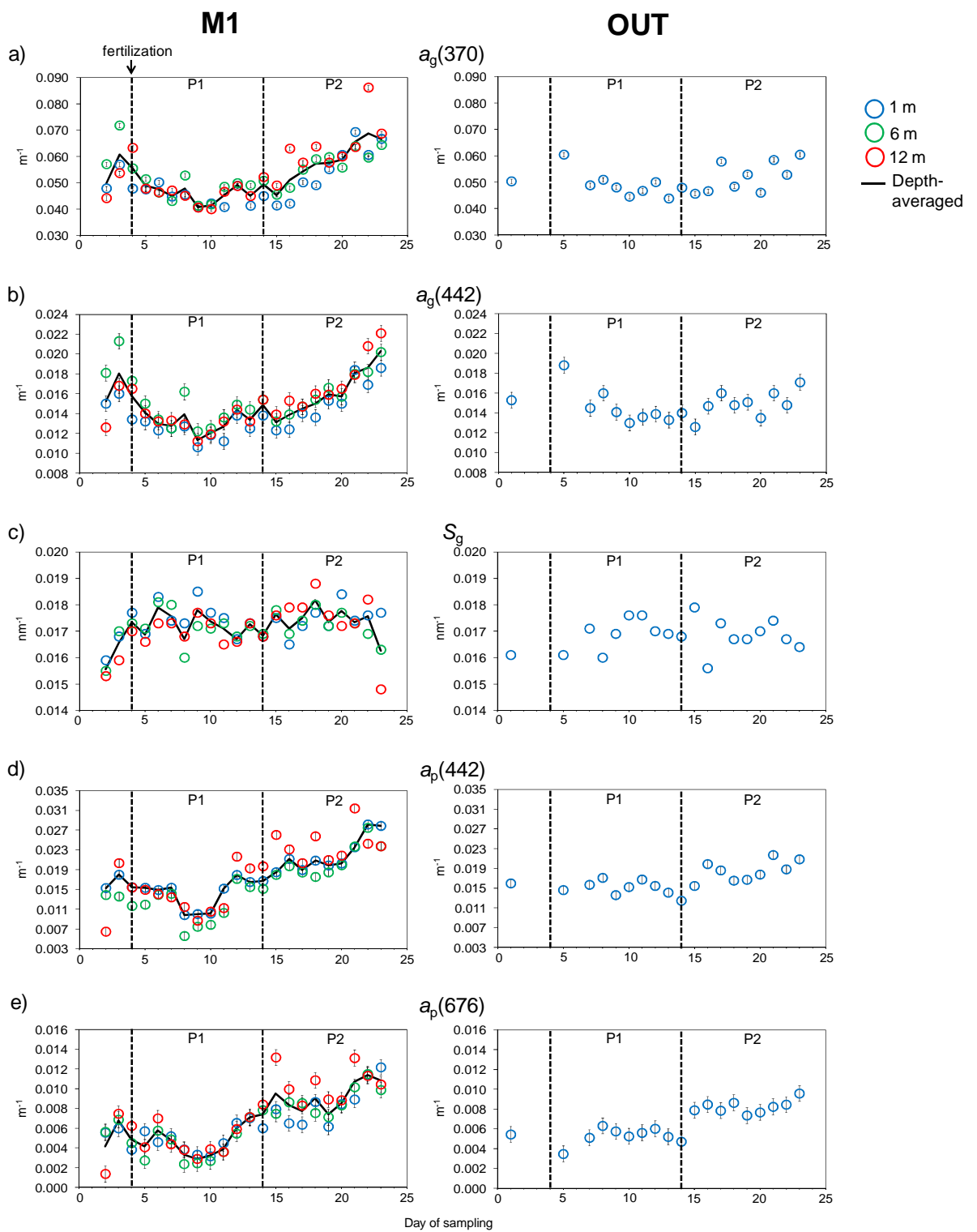
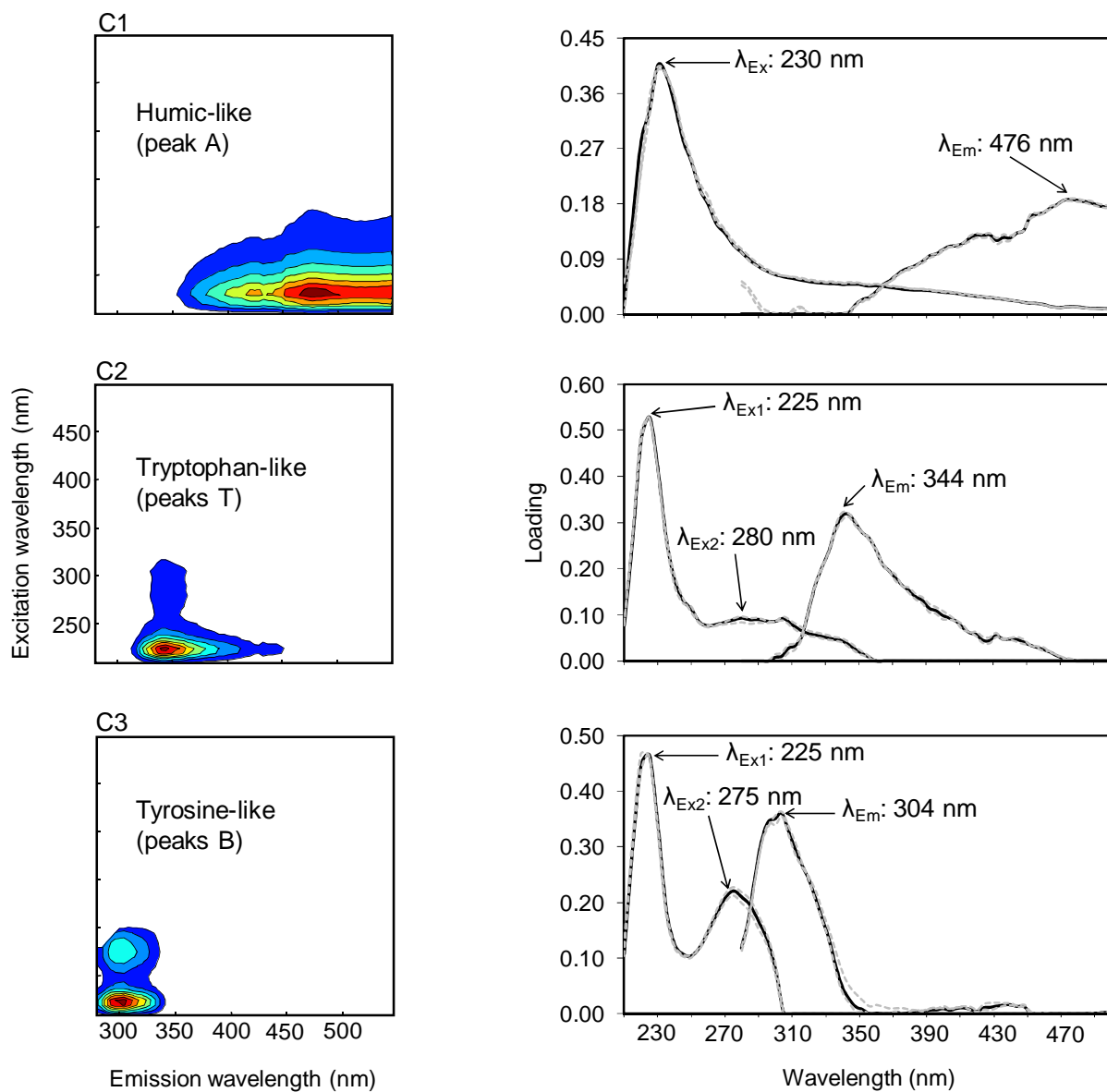


Figure 6

1355



1356

1357

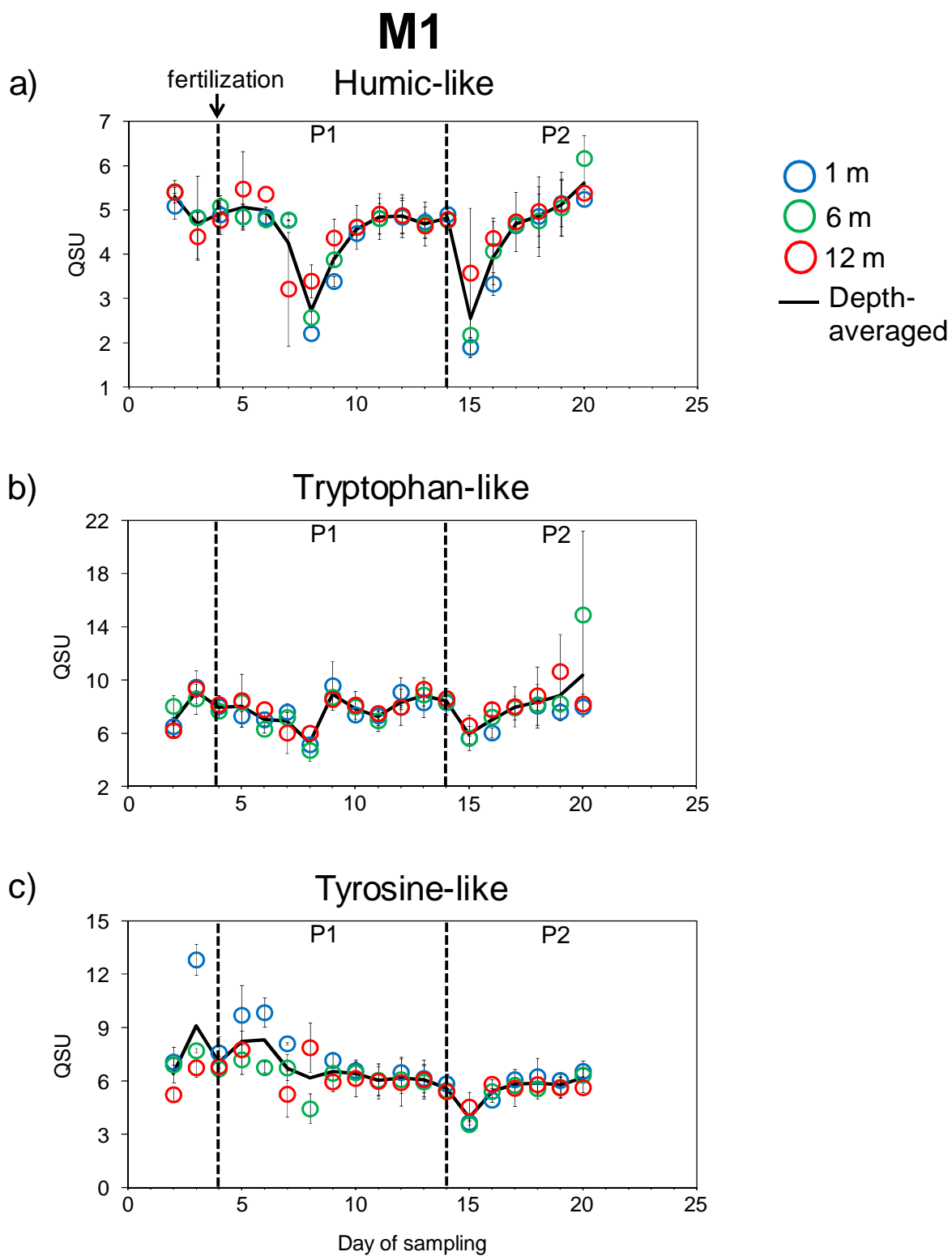
1358

1359

1360

1361

Figure 7



1363

1364

1365

1366

Figure 8

1367
1368
1369
1370
1371
1372
1373
1374
1375
1376
1377
1378
1379
1380
1381
1382
1383
1384
1385
1386
1387
1388
1389
1390
1391
1392
1393
1394
1395
1396
1397
1398
1399

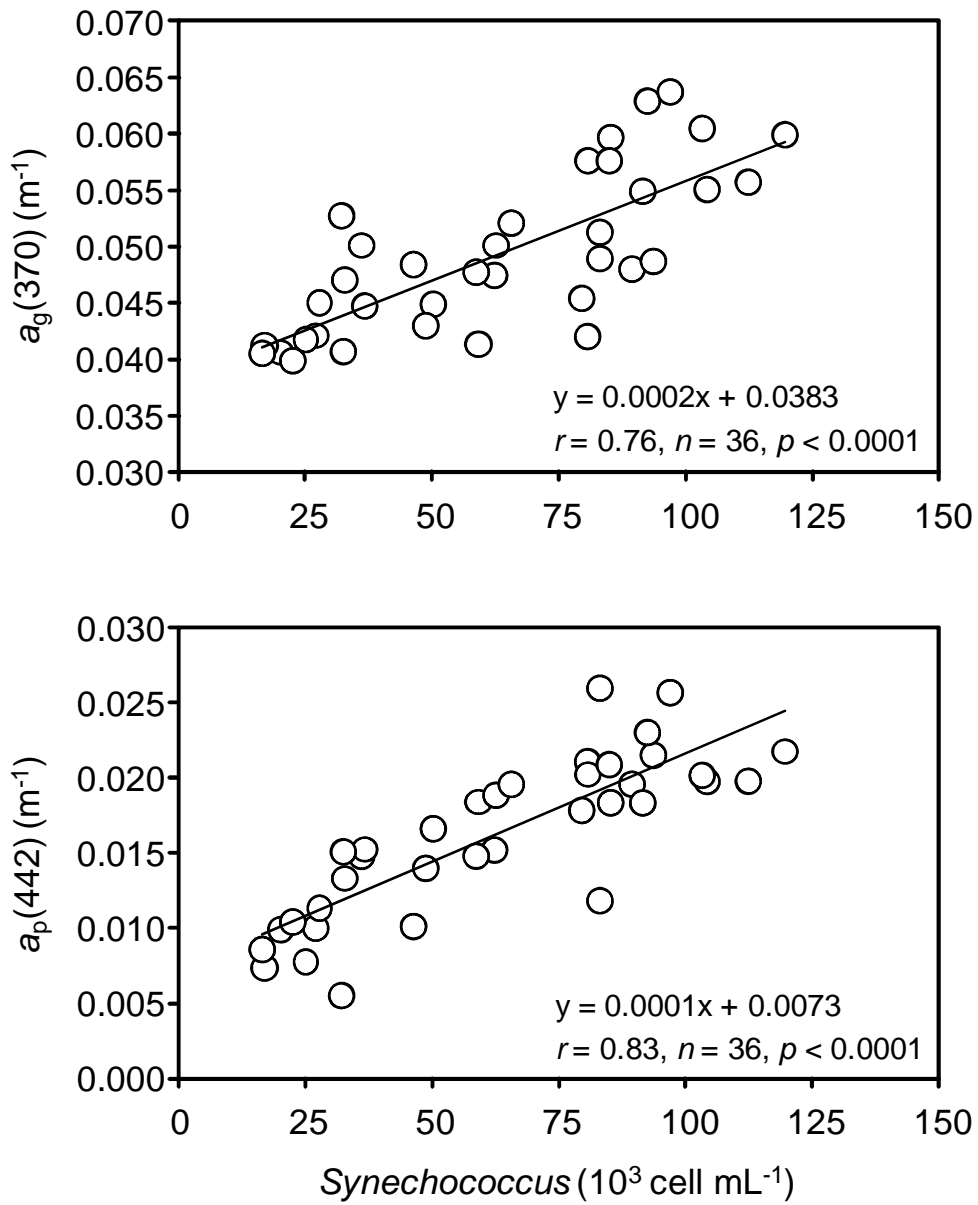


Figure 9